Nanoparticle-Conjugated TLR9 Agonists Improve the Potency, Durability, and Breadth of COVID-19 Vaccines

Ben S. Ou[‡,1], Vittoria C.T.M. Picece[‡,2,3], Julie Baillet[2,4], Emily C. Gale[5], Abigail E. Powelll[5,6], Olivia M. Saouaf[2], Jerry Yan[1], Hector Lopez Hernandez[2], Eric A. Appel[1,2,6,7,8]*

1. Department of Bioengineering, Stanford University, Stanford, CA 94305, USA

2. Department of Materials Science & Engineering, Stanford University, Stanford, CA 94305, USA

3. Department of Chemistry and Applied Biosciences, ETH Zurich, Zurich 8093, Switzerland

4. CNRS, Bordeaux INP, LCPO, University of Bordeaux, Pessac, 33600 France

5. Department of Biochemistry, Stanford University School of Medicine, Stanford, CA 94305, USA

6. Stanford ChEM-H, Stanford University, Stanford, CA 94305, USA

7. Department of Pediatrics - Endocrinology, Stanford University School of Medicine, Stanford, CA 94305, USA

8. Woods Institute for the Environment, Stanford University, Stanford CA 94305, USA

‡ These authors contributed equally to this work.

* Corresponding Author: eappel@stanford.edu

KEYWORDS

Vaccines, Hydrogels, SARS-CoV-2, Drug delivery, Immunoengineering

ABSTRACT

Development of effective vaccines for infectious diseases has been one of the most successful global health interventions in history. Though, while ideal subunit vaccines strongly rely on antigen and adjuvant(s) selection, the mode and timescale of exposure to the immune system has often been overlooked. Unfortunately, poor control over the delivery of many adjuvants, which play a key role in enhancing the quality and potency of immune responses, can limit their efficacy and cause off-target toxicities. There is critical need for new adjuvant delivery technologies to enhance their efficacy and boost vaccine performance. Nanoparticles (NPs) have been shown to be ideal carriers for improving antigen delivery due to their shape and size, which mimic viral structures, but have been generally less explored for adjuvant delivery. Here, we describe the design of self-assembled poly(ethylene glycol)-*b*-poly(lactic acid) nanoparticles decorated with CpG, a potent TLR9 agonist, to increase adjuvanticity in COVID-19 vaccines. By controlling the surface density of CpG, we show that intermediate valency is a key factor for TLR9 activation of immune cells. When delivered with the SARS-CoV-2 spike protein, CpG NP adjuvants greatly improve the magnitude and duration of antibody responses when compared to free CpG, and result in overall greater breadth of immunity against variants of concern. Moreover, encapsulation of CpG NPs into injectable polymeric-nanoparticle (PNP) hydrogels enhance the spatiotemporal control over co-delivery of CpG NP adjuvant and spike protein antigen such that a single immunization of hydrogel-based vaccines generates comparable humoral responses as a typical prime-boost regimen of soluble vaccines. These delivery technologies can potentially reduce the costs and burden of clinical vaccination, both of which are key elements in fighting a pandemic.

INTRODUCTION

Vaccines are among the most effective medical advancements in history and are estimated to save 2.5 million lives worldwide annually.[1] Unfortunately, an abundance of infectious diseases – including many rapidly mutating viral pathogens such as HIV, influenza, and SARS-CoV-2 – still do not have sufficiently effective vaccines capable of providing broad and durable protection for a global population. To date, roughly one million people die each year from flu and HIV and COVID has killed more than 6.5 million people since its arrival three years ago[2], highlighting the continuing threat of pandemic viruses and a critical need for improved vaccine technologies.

Among the common types of vaccines used in the clinic, subunit vaccines offer excellent safety, stability, scalability, and worldwide manufacturing capabilities, as well as more widely available storage conditions compared to mRNA-based vaccines.[3] Subunit vaccines contain protein antigens, which direct the antibody response to a specific foreign substance, along with one or more immune stimulating additives commonly referred to as adjuvants. These adjuvant materials have been shown to play a key role in enhancing the body's immune response to a pathogen and therefore vaccine efficacy. Yet, there is a growing need for new approaches to augment adjuvant potency and enhance the quality and durability of immune responses.[4] Some of the most widely used clinical adjuvants include aluminum salt-based adjuvants (Alum) and squalene-based oil-in-water emulsions such as MF59 and AS03, though the specific mechanism of action of these adjuvants is poorly understood.[5] There are also several molecular adjuvants which trigger innate immune cell activation through signaling of pattern recognition receptors (PRR), including toll-like receptor agonists (TLRas) such as oligodeoxynucleotide CpG ODN (TLR9 agonist) and MPL (TLR4 agonist). CpG, for example, has been shown to increase immune responses by strongly

activating innate immune cells as the CpG motifs mimic the activity of bacterial DNA.[6] Specifically, CpG triggers intracellular signaling leading to the activation of antigen presenting cells (APCs) such as macrophages and dendritic cells (DCs) and B cells, as well as the production of chemokines and cytokines, enhancing both innate and adaptive immune responses.[7-14] CpG is included in the Hepatitis B vaccine Heplisav B (FDA approved in 2017), and is also currently being evaluated clinically in multiple SARS-CoV-2 vaccines.[15]

To maximize the activation of innate immune cells while minimizing systemic toxicities,[16, 17] significant efforts have focused on localizing TLR agonists to the injection site and lymph nodes (LNs). Nanoparticles (NPs) have been extensively explored as delivery carriers due to their modularity, scalability, biocompatibility, and ability to overcome spatiotemporal challenges associated with conventional delivery methods.[16-29] NPs between 20 and 100 nm[30-35] efficiently drain through the lymphatic system into the LNs[30, 31, 36] where they are directly taken up by LN-resident APCs[37] without requiring specific cell targeting ligands. Moreover, recent studies have reported that covalently conjugating TLRa molecules to polymer NPs results in a significant increase in both antibody production and induction of cytotoxic T-cells.[17] Similarly, other studies have leveraged particle technologies to present multiple adjuvant molecules on their surface in order to improve the potency of the adjuvant response.[17, 38-40] A growing body of work demonstrated that immune cells require precise spatial and temporal cues to drive specified responses, supporting the idea that spatiotemporal control of vaccines can have a profound effect on the magnitude and quality of the immune response.[41-50]

The precise spatiotemporal control of vaccines can also be achieved by localized slow delivery of vaccine components. Recent proof-of-concept studies have shown that sustained release of an HIV vaccine through implantable osmotic pumps led to greatly improved quality of vaccine responses, such as durable germinal center (GC) responses, high antibody titers, and development of better virus neutralization compared to standard soluble administration of the same vaccine.[47] Similarly, microneedles and injectable hydrogels have been widely used as slow vaccine delivery platforms.[29] Our group has developed injectable polymer-nanoparticle (PNP) hydrogels for prolonged co-delivery of subunit vaccine components.[44, 51-55] We have demonstrated that PNP hydrogels can provide sustained release of vaccine cargos over the course of weeks, while prolonging the GC reaction and improving antibody affinity by more than 1000-fold compared to soluble vaccine formulation.[44, 56, 57]

In the current study, we sought to optimize the delivery of CpG to improve the potency by developing a nanoparticle-based adjuvant construct. We chemically conjugated the CpG adjuvant to poly(ethylene glycol)-*b*-poly(lactic acid) (PEG-*b*-PLA) NPs of approximately 50 nm in size, allowing for efficient, passive and direct transport to the LNs (Figure 1). We showed not only was CpG activity unaffected by the conjugation to the NPs, but also precise tuning of the CpG valency on the NPs surface enabled control of the potency of the elicited immune response *in vitro*. Moreover, these modifiable adjuvant-NPs can be embedded into PNP hydrogels for sustained exposure of vaccine adjuvants to improve immune responses. In this regard, we compared the adjuvanticity of soluble CpG, CpG-functional NPs, and PNP hydrogels containing CpG-functional NPs (CpG NP hydrogel) in vivo when part of a COVID-19 subunit vaccine using the SARS-CoV-2 spike protein as antigen. We showed that a single immunization of CpG NP hydrogel as well as

a prime-boost soluble CpG NP vaccine demonstrated superior anti-spike antibody titers and broader antibody responses against immune-evading variants. Overall, we report the facile design of a broadly implementable CpG NP platform that can improve adjuvant potency leading to increased breadth and durability of vaccines.

RESULTS AND DISCUSSION

Synthesis and characterization of CpG NPs

We conjugated the TLR9 adjuvant CpG to PEG-*b*-PLA NPs to improve its stability, its targeting to LNs and its uptake by APCs (Figure 2). We have previously described the synthesis of azide-terminated PEG-*b*-PLA (N_3-PEG-*b*-PLA) block copolymers using organocatalytic ring-opening polymerization (ROP) and their self-assembly in core-shell types NPs.[26, 27, 51, 52, 58, 59] DBCO-modified CpG was tethered on the surface of N_3-PEG-*b*-PLA NPs using copper-free strain-promoted cycloaddition (Figure 2A). Conversions higher than 90% were obtained with a threefold molar excess of DBCO-CpG with respect to the azide functionality on the NPs (Figure S1). Different valencies of TLR agonists on NPs have been shown to influence the magnitude and persistence of innate immune activation by leading to higher expression of co-stimulatory molecules.[17, 59] Therefore, manipulating the density of the CpG adjuvant molecules on the surface of the PEG-*b*-PLA NPs could potentially improve the potency of adjuvant responses.[29, 38, 59] A series of NPs with increasing CpG valencies on the surface were obtained by controlling the number of azide functionalities when physically mixing different ratios of N_3-PEG-*b*-PLA and PEG-*b*-PLA (i.e., 10%, 20%, 30% and 50%; SI). The resulting CpG NPs were purified via size exclusion chromatography and the purity was assessed by size exclusion chromatography and gel electrophoresis (Figures S2, S3). The conjugation did not affect the physical and colloidal

properties of the NPs and successful CpG functionalization was confirmed by an increase in UV absorbance, hydrodynamic diameter, and the zeta potential (Figures 2B, 2C, 2D). CpG NPs were found to have hydrodynamic diameters between 56 to 62 nm (Table S1), which is within the size range known to demonstrate improved trafficking to LNs[30,31,36] while avoiding immediate partitioning of free CpG into the blood stream and therefore reducing systemic toxicities (Figures 2C, S4). Moreover, the negatively charged phosphorothioate backbone of CpG induced an increase of negative charge on the NPs, therefore increasing the colloidal stability of the NPs (Figure 2D).

In vitro evaluation of CpG NPs potency

To ensure that CpG conjugation to the NPs did not impair the biological activity and immunogenicity of the adjuvant, RAW-Blue transgenic mouse macrophage cells were used to quantify TLR9 activation (Figure 3a). The cells were incubated with either CpG NPs or soluble CpG. Additionally, this *in vitro* assay was used to evaluate the impact of CpG valency on the NPs and the effect of valency on the potency of innate immune cell activation. In these assays, Raw-Blue cells were incubated for 21 h with either soluble CpG, plain PEG-*b*-PLA NPs, or CpG-conjugated NPs (with valencies of 10%, 20%, 30%, 50%) at a range of CpG concentrations (3.1–29 μg/mL) to generate concentration-dependent activation curves (Figure 3B). To ensure a correct and consistent dosing of CpG NPs throughout different experiments, we constructed a standard curve for the CpG NPs (Figure S5). From the dilution curves, we then determined the EC_{50} values (Figure 3C). We observed that CpG density influenced the resulting EC_{50} values and therefore their potency. 30% CpG NP generated EC_{50} value that was 66% lower (log EC_{50} = 1.2 μg/mL) than the EC_{50} value (log EC_{50} = 1.7 μg/mL) of the 10% CpG NP. Furthermore, 30% CpG NP resulted in the lowest EC_{50} value compared to all other valencies and behaved similarly to free

CpG (log EC_{50} = 1.15 μg/mL). Interestingly, 50% valency resulted in the highest EC_{50} value (log EC_{50} = 2.1 μg/mL) compared to the other NPs, suggesting a low level of TLR9 activation. The reduction in potency observed with the highest valency 50% CpG NPs could be due to steric hindrances and a highly negatively charged surface which, by surpassing the critical threshold for charge density, thereby decreasing CpG accessibility. Based on these results, 30% CpG NPs were identified as the most promising CpG NPs adjuvant to promote high magnitude and persistent immune activation and further tested in an *in vivo* vaccine study with a SARS-CoV-2 antigen. All subsequent studies were thus performed with 30% CpG NPs and simply denoted as CpG NPs. These data demonstrate that we were able to synthesize stable CpG NPs of different valencies, and that the intermediate CpG valency on 30% CpG NPs activated TLR9 with similar potency to free CpG *in vitro*.

Formation of CpG NP hydrogels and rheological characterization

Recent studies have highlighted the importance of sustained delivery in vaccines to prolong GC responses leading to improved breadth and affinity of antibody responses.[47, 60] We have previously described the development of tunable and injectable PNP hydrogels able to encapsulate physiochemically diverse vaccine components such as antigens and adjuvants and to provide sustained co-delivery over extended periods of time.[44, 56, 57, 61] We hypothesized that these unique characteristics could be coupled with the newly designed CpG NPs featuring improved potency and *in vivo* trafficking properties to further enhance the vaccine response. PNP hydrogels can be easily formed by mixing aqueous solutions of hydrophobically modified hydroxypropyl methylcellulose derivatives (HPMC-C_{12}) and biodegradable PEG-*b*-PLA NPs (Figure 4A).[44, 51, 54, 55] After mixing, dynamic and multivalent non-covalent interactions form between the HPMC-C_{12}

and the PEG-*b*-PLA NPs yielding dynamic crosslinks that lead to the formation of robust physical hydrogels (Figure 4B). These supramolecular hydrogels exhibit solid-like properties under static conditions, liquid-like behaviors under high shear, and rapid self-healing after succession of shear, allowing them to be readily injected through standard needles and form solid depots after injection.

Vaccine components, including both adjuvants and antigens, can easily be loaded within the hydrogel network by simply mixing into the aqueous stock solutions during hydrogel manfacturing.[44] To ensure that CpG-conjugation to the NPs did not influence the mechanical properties of PNP hydrogels, we compared rheological properties of PNP hydrogels comprising CpG NPs with standard hydrogel formulations (Figure 4C-G). We specifically investigated PNP hydrogel formulations comprising 2wt% HPMC-C_{12} and 10wt% NPs (containing a mixture of plain PEG-*b*-PLA NPs and CpG NPs), which is denoted PNP-2-10. Frequency-dependent oscillatory shear experiments were conducted within the linear viscoelastic regime (LVER) of the materials to measure their viscoelastic response. These experiments indicated that the introduction of CpG NPs did not significantly alter the PNP hydrogel's mechanical properties. Both formulations with and without CpG NPs showed solid-like properties within the explored frequency range in which the storage (G') modulus was greater than the loss (G'') modulus (Figure 4C and 4D). We also evaluated the yielding response of the hydrogels, which is an important characteristic for injectability and depot formation,[62] using amplitude-dependent oscillatory shear experiments and stress-controlled flow experiments. Yield stress values of ~935 Pa were measured by stress-controlled flow sweeps (Figure 4E). Further, the flow sweeps demonstrated that these materials exhibit a high degree of shear-thinning, whereby the measured viscosities decreased several orders of magnitude with increasing shear (Figure 4F).

Step-shear experiments were also conducted by interchanging in a stepwise fashion between low (0.1 1/s) and high (10 1/s) shear rates to determine self-healing behaviors of the hydrogels. The viscosity was observed to decrease by several orders of magnitude upon application of high shear rates, and rapidly and completely recovered when subjected to low shear rates (Figure 4G). From these observations, we confirmed that the inclusion of CpG NPs did not alter the rheological characteristics of PNP hydrogels. We also showed these CpG NP comprising hydrogels can be readily injected through high-gauge needles (Figure 4Biv) and maintain a robust structure after injection to allow for the formation of a robust depot *in vivo*.[44, 63]

Vaccine cargo dynamics in PNP hydrogels

Vaccine components, including both antigens and adjuvants, typically exhibit highly distinct physiochemical properties that pose a challenge for their controlled and sustained delivery. These components can have extremely different polarities, charges, molecular weights, and hydrodynamic radii (R_H) influencing that may impact their encapsulation and diffusivity within a hydrogel network.[44] Given the hydrophilicity and smaller molecular size of soluble CpG compared to the mesh size of a typical PNP-2-10 hydrogel formulation, soluble CpG has been shown previously to rapidly diffuse out of these hydrogel (half-life of release ~2.5 days).[57, 64, 65] We therefore hypothesized that sustained co-delivery of CpG NPs and the SARS-CoV-2 spike protein (S), whose hydrodynamic sizes are expected to be much larger than the mesh size of the hydrogel, can be achieved with these materials. To evaluate this hypothesis, PNP-2-10 hydrogels were prepared with CpG NPs (R_H ~ 30 nm) and loaded with S protein (R_H = 12 nm, M_w = 139 kDa). To characterize the dynamics of vaccine diffusion within the PNP hydrogels, we performed fluorescence recovery after photobleaching experiments (FRAP) (Figure 5).

We fluorescently labeled both of the main PNP hydrogel components (both the NPs and HPMC-C_{12}) and the S protein antigen, and the diffusivity of each component was assessed in distinct experiments to isolate the individual diffusivity effects. From the fluorescence recovery behavior of these molecules, we determined diffusivities, *D,* of hydrogel structural components (HPMC-C_{12}), CpG NPs, and spike protein (n.b. using Eq. 1). FRAP measurements showed that the hydrogel network dramatically reduced the cargo diffusivity of the S protein by over 30-fold, with a measured diffusivity of D_{spike} = 0.64 μm^2/s, compared to the antigen's free diffusivity in PBS, which was determined to be D = 20.22 μm^2/s by DLS (n.b. using Eq. 2; Figure 5C). Moreover, the self-diffusion of the PNP matrix, D_{gel}, was determined by measuring the diffusivity of the HPMC-C_{12} within the fully formulated hydrogel and found to be D_{gel} = 0.98 μm^2/s. The diffusivity of CpG NPs (D_{NP} = 0.68 μm^2/s) and S protein in the hydrogel (D_{spike} = 0.64 μm^2/s) were very similar to the self-diffusion of the PNP matrix, resulting in a diffusivity ratio (D_{cargo}/D_{gel}) close to 1 for both components (Figure 5D). These results indicate that both cargos, despite their physiochemical differences, are immobilized by the hydrogel's polymeric network and are diffusing at rates limited by the self-diffusivity of the hydrogel matrix, which arises due to the continuous rearrangement of the dynamic physical PNP network bonds.

Immunogenicity of COVID-19 vaccines comprising CpG NP adjuvants

We next investigated the immunogenicity of COVID-19 vaccines comprising S protein antigen and either soluble CpG or CpG NPs adjuvants, as well as CpG NP hydrogels. The S protein has been one of the most promising antigens used in SARS-CoV-2 subunit vaccine candidates and forms the basis for most clinical vaccines. The spike protein contains the receptor binding domain

(RBD) that recognizes the cell surface receptor ACE2 and which is vital for viral fusion and infection. In these experiments, we subcutaneously (s.c.) immunized 8 weeks old C57BL/6 mice with vaccines containing 10 μg of S antigen and adjuvanted with either soluble CpG (20 μg), CpG NPs (containing an equivalent of 20 μg of CpG), or PEG-PLA NPs as a vehicle control. These soluble vaccine groups received a prime immunization at week 0 and a boost immunization on week 3, with sera collected weekly from weeks 0-10 (Figure 6A). As we have previously demonstrated robust humoral responses with a single immunization of SARS-CoV-2 RBD hydrogel vaccines,[57] we also evaluated a single hydrogel immunization comprising S antigen (20 μg) and CpG NP adjuvant (40 μg) administered s.c. on week 0. As with the prime-boost soluble vaccines, sera were collected weekly at weeks 0-10. Thus, these single immunization PNP hydrogel vaccines contained the same total dose of antigen and adjuvant as the complete prime-boost soluble vaccine regimens.

High systemic levels of inflammatory cytokines are associated with toxicity in both rodents and humans,[66, 67] therefore we assessed inflammatory cytokines IFN-α (Figure S6A) and TNF-α (Figure S6B) at 3 h and 24 h after immunization to ensure the vaccines did not drive systemic cytokine responses posing a potential safety risk. No increased cytokine levels were detected (less than 20 pg/mL) across all treatment groups, including the PNP hydrogel group that contained a double vaccine dose. These findings suggest all treatments are well tolerated.

To assess humoral immune responses, spike-specific immunoglobulin G (IgG) endpoint antibody titers were quantified weekly throughout the experiment. One week post prime immunization, the endpoint titers were below the detection limit for all of the soluble vaccine

groups (except for one mouse in the CpG NPs group) but were sufficiently high in the CpG NP hydrogel group to suggest all animals had seroconverted (Figure 6B, Figure S7B, $P < 0.0001$ for comparison of hydrogel group to all other groups). This observation indicates more rapid seroconversion from IgM to IgG following hydrogel-based immunization, implying quicker disease protection that is highly desirable in a pandemic setting.[56, 57] CpG NP hydrogel vaccines elicited higher anti-spike IgG endpoint titers than all soluble vaccines over the first three weeks prior to boost immunization in these groups.

Following boost immunization, the CpG NP group elicited endpoint titers nearly 2 orders of magnitude higher than those elicited by the soluble CpG group ($P < 0.001$ for all time points post-boost). We also observed significantly higher titers for the CpG NP group compared to all other control groups (with $P < 0.05$ for all time points post-boost). Similarly, the prime-only CpG NP hydrogel vaccine group elicited comparable endpoint titers to prime-boost CpG NP vaccine group from week 3 to the end of the study ($P > 0.05$ at all timepoints; $P = 0.99$ on D70). Notably, significantly increased area under the curve (AUC) of endpoint titers was observed over the entire study period for both the prime-boost CpG NP group and the CpG NP hydrogel group compared to the soluble CpG group and PEG-PLA NP control group (Figure 6C, Figure S7C). Additionally, consistent with our previous findings, we also observed smaller variability in titer across animals for the prime-only CpG NP hydrogel group compared to all of the prime-boost soluble vaccines evaluated, which is an important characteristic for ensuring sufficient immunity among all members of a broad population. Overall, these findings demonstrate that CpG NP adjuvants significantly improve humoral immunity of S-based vaccines compared to soluble CpG adjuvants,

and that sustained co-delivery of CpG NP adjuvants and S antigen within PNP hydrogels allows for prime-only single immunization with similarly improved humoral immune responses.

In addition to evaluating humoral responses to the homologous wildtype (WT) SARS-CoV-2 spike variant, we assessed whether the newly designed vaccines can generate broad protection against emerging SARS-CoV-2 variants such as Beta (B.1.351), Delta (B.1.617.2), and Omicron (B.1.1.529) variants by determining the total IgG endpoint titers against these variants. Across all vaccine groups, decreased titers against all three variants of concern were observed, which is consistent with the known immune-evasion of these variants.[68] Yet, both prime-boost CpG NP vaccines and prime-only CpG NP hydrogel vaccines elicited significantly higher endpoint titers against these three variants of concern compared to prime-boost soluble CpG vaccines and prime-boost PEG-PLA NP control vaccines (Figure 6D, Figure S7D; $P < 0.05$ for all comparisons). Notably, the endpoint titers against the three variants elicited by prime-boost CpG NP vaccines and prime-only CpG NP hydrogel vaccines remained higher than WT endpoint titers produced by the prime-boost soluble CpG vaccines. Specifically, CpG NP and CpG NP hydrogel vaccines elicited anti-Omicron titers equal to the anti-WT titers elicited by the soluble CpG control vaccines ($P > 0.999$ for comparison of both CpG NP group and CpG NP hydrogel group's anti-Omicron titers to soluble CpG group's anti-WT titers). Moreover, we observed a 28% and 24% drop in anti-Omicron titers for prime-boost soluble CpG and CpG NP groups compared to each group's anti-WT titers, respectively (Figure S8). These decreases were greater than that determined for the CpG NP hydrogel group, which demonstrated only a 19% drop in anti-Omicron titers compared to anti-WT titers ($P = 0.16$ and $P = 0.67$ for the comparison of the titer reduction of the CpG NP hydrogel group compared to the CpG NP group and the soluble CpG group, respectively). In sum, both CpG

NP and CpG NP hydrogel vaccines demonstrated enhanced breadth of humoral immunity against SARS-CoV-2 variants of concern than soluble CpG vaccines.

We next evaluated IgG isotypes at week 7 of the study to assess immune signaling and antibody class-switching following each vaccination. We were especially interested in determining the elicitation of IgG1 and IgG2c antibody responses as these are respectively associated with Th2- and Th1-dominated immune responses.[69] We found both CpG NP and CpG NP hydrogel vaccines exhibited elevated IgG1 endpoint titers compared to other groups (Figure 7A, $P < 0.05$). Moreover, all groups containing CpG showed elevated IgG2c endpoint titers compared to the PEG-PLA NP control group (Figure 7B, Figure S9B). When assessing the ratio of IgG2c to IgG1, all CpG containing groups were found to elicit an IgG2c/IgG1 ratio close to 1, suggesting balanced Th1 and Th2 responses (Figure 7C). This observation is consistent with reported studies comparing CpG to other clinical adjuvants such as Alum.[70-72] Despite previously observing generally more Th2-skewed responses in PNP hydrogels compared to soluble vaccine counterparts,[44, 56, 57] CpG NP hydrogels maintained a more balanced response. In the context of COVID-19 infection, clinical studies have found that a rapid onset of a Th1 response resulted in less severe disease outcomes, whereas Th2-skewed responses were associated with greater lung inflammation and higher patient mortality.[73, 74] The role of the CpG NP adjuvants in inducing potent Th1 responses may be especially advantageous as a COVID-19 vaccine adjuvant. Future studies will reveal the degree to which CpG NP adjuvants impact cell-mediated responses, including induction of antigen-specific cytotoxic CD8+ T cells.

SARS-CoV-2 Spike-Pseudotyped Viral Neutralization Assay

We also sought to evaluate the neutralizing activity of the sera from each vaccine group using lentivirus pseudotyped with SARS-CoV-2 spike and determining the inhibition of viral entry into HeLa cells overexpressing the angiotensin-converting enzyme 2 (ACE2) surface receptor (Figures 6A). We first measured the neutralizing activity of sera at week 3 of the study (pre-boost for soluble vaccines) at a single serum dilution of 1:50 (Figure 8A, Figure S10A). Sera from mice immunized with soluble vaccines was found to have at least 50% infectivity, with sera from the PEG-PLA NP control and soluble CpG vaccine groups having negligible effect on viral infectivity. On the other hand, sera from mice immunized with CpG NP hydrogels protected cells from infection ($P < 0.0001$ for comparison of infectivity of CpG NP hydrogel to all other vaccine groups). This finding suggests that the CpG NP hydrogel vaccines rapidly generate robust neutralizing activity following a single immunization.

We then measured the neutralizing activity of sera at week 5 of the study (two weeks post-boost for soluble vaccines) from all vaccine formulations at a single dilution of 1:50 (Figure 8B, Figure S10B). We determined that sera from soluble vaccine groups resulted in an infectivity less than 50% only after boosting, while sera from the single-immunization CpG NP hydrogel vaccine group again exhibited protection against infection. We then assayed a range of sera concentrations from all groups to determine the half maximal inhibition of infectivity (IC_{50}) (Figure 8C-F, Figure S10C-D). The prime-boost CpG NP vaccine group was found to have the most potent neutralization (IC_{50} ~$1.5x10^4$), followed the prime-only CpG NP hydrogel group (IC_{50} ~ $2.7x10^3$). Even though the soluble vaccine groups had just received a booster vaccination 2 weeks prior, the measured IC_{50} from the single-immunization CpG NP hydrogel group was comparable to the other prime-boost soluble vaccine groups ($P > 0.05$ comparing all groups to the CpG NP hydrogel group).

Overall, we determined that a single immunization of CpG NP hydrogel vaccines was similarly effective as a prime-boost immunization regimen with soluble CpG NP vaccines in terms of overall antibody titer, durability of titer responses, breadth of antibody responses, balanced Th1 and Th2 responses, as well as neutralization activity. Further, vaccines formulated with CpG NPs (e.g., both prime-only CpG NP hydrogel and prime-boost CpG NP vaccines) demonstrated superior overall humoral responses compared to vaccines comprising soluble CpG as an adjuvant.

CONCLUSIONS

In conclusion, we have developed a potent adjuvant NP platform allowing enabling the presentation of TLR9 agonists on the surface of PEG-*b*-PLA NPs. Our facile synthetic and formulation approach allows for precise control of the valency of adjuvant distribution on the NP surface. We showed that the density of CpG presentation strongly influenced the activation of TLR9, and that an intermediate density of CpG on the NP surface (e.g., 30% CpG NPs) exhibited the greatest potency *in vitro* compared to soluble CpG. When these CpG NPs were used as adjuvants in candidate COVID-19 vaccines using the SARS-CoV-2 spike protein, we found that they elicited superior humoral responses compared to soluble CpG adjuvants. Indeed, vaccines comprising CpG NP adjuvants elicited more potent and sustained antibody titers, more robust breath of recognition of immune-evading variants of concern, balanced Th1 to Th2 responses, and more strongly neutralizing antibody responses than soluble CpG. These promising CpG NP adjuvants were further evaluated within PNP hydrogels to enhance the spatiotemporal control of vaccine delivery. Embedding of CpG NPs within PNP hydrogels was found to negligibly impact the rheological properties compared to standard PNP hydrogels. Additionally, we confirmed the

immobilization of both CpG NPs and SARS-CoV-2 spike protein in the hydrogel's network results in similar diffusive properties, despite their physicochemical differences, thereby enabling sustained co-delivery of both vaccine components. Importantly, a single immunization of CpG NP hydrogels generated comparable humoral responses to a prime-boost regimen of CpG NP soluble vaccines. The promising results of single-immunization CpG NP hydrogel vaccines could reduce clinical vaccination costs, increase patient compliance, and ultimately result in more rapid uptake of vaccines and higher vaccination rates, which are all key elements when fighting against a rapidly evolving pandemic.

EXPERIMENTAL SECTION

Materials

Poly(ethylene glycol)methyl ether 5000 Da (PEG), Poly(ethylene glycol)α-hydroxy-ω-azido terminated 5000 Da (N_3-PEG-OH), 3,6-Dimethyl-1,4-dioxane-2,5-dione (Lactide), 1,8-diazabicyclo(5.4.0)undec-7-ene (DBU, 98%), (Hydroxypropyl)methyl cellulose (HPMC, meets USP testing specifications), *N,N*-Diisopropylethylamine (Hunig's base), *N*-methyl-2-pyrrolidone (NMP), 1-dodecyl isocyanate (99%), mini Quick Spin Oligo columns (Sephadex G-25 Superfine packing material), Sepharose CL-6B crosslinked, bovine serum albumin (BSA), were purchased from Sigma-Aldrich. CpG-C 2395 (5'-TCGTCGTTTTCGGCGCGCGCCG-3') oligonucleotide, Aluminum hydroxide gel (Alhydrogel adjuvant 2%), zeocin were purchased from InvivoGen. Amino CpG-C 2395 (5'Amino Modifier C_6, 5'-NH_2-TCGTCGTTTTCGGCGCGCGCCG-3') were purchased from Integrated DNA Technologies (IDT). Dibenzocyclooctyne-PEG4-*N*-hydroxysuccinimidyl ester (DBCO-PEG4-NHS ester) and Alexa Fluor 647 DBCO (AFDye 647 DBCO) were purchased from Click Chemistry Tools. Dulbecco's modified Eagle's medium (DMEM, Gibco), phosphate buffered saline (PBS pH 7.4, Gibco) and Invitrogen E-Gel EX Agarose Gels 4% were purchased from Thermo Fisher Scientific. Heat Inactivated fetal bovine serum (HI-

FBS) was purchased from Atlanta Biologicals. IFN-α cytokine enzyme-linked immunosorbent assay (ELISA) kit was purchased from PBL Assay Science, and the TNF-α cytokine ELISA kits was purchased from R&D Systems (Fisher Scientific). Goat anti-mouse IgG Fc secondary antibody (A16084) HRP (Horseradish peroxidase) was purchased from Invitrogen. Goat anti-mouse IgG1 and IgG2c Fc secondary antibodies (ab97250, ab97255) HRP were purchased from abcam. 3,3',5,5'-Tetramethylbenzidine (TMB) ELISA Substrate, high sensitivity was acquired from Abcam. HIS Lite Cy3 Bis NTA-Ni Complex was purchased from AAT Bioquest. Unless otherwise stated, all chemicals were used as received without further purification.

Synthesis of PEG-*b*-PLA

PEG-*b*-PLA was prepared as previously reported [52]. Prior to use, commercial lactide was recrystallized in ethyl acetate and DCM was dried via cryo distillation. Under inert atmosphere (N_2), PEG-methyl ether (5 kDa, 0.25 g, 4.1 mmol) and DBU (15 µL, 0.1 mmol) were dissolved in 1 mL of anhydrous DCM. Lactide (1.0 g, 6.9 mmol) was dissolved under N_2 in 3 mL of anhydrous DCM. The lactide solution was then quickly added to the PEG/DBU mixture and was allowed to polymerize for 8 min at room temperature. The reaction was then quenched with an acetic acid solution and the polymer precipitated into a 1:1 mixture of ethyl ether and hexanes, collected by centrifugation and dried under vacuum. NMR spectroscopic data, Mn and Dispersity were in agreement with those previously described.

Synthesis of azide PEG-*b*-PLA

Azide-PEG-b-PLA was synthesized according to the literature.[59, 61] Prior to use, DCM was dried using 3-4 Å molecular sieves and N_3-PEG-OH was dried under vacuum overnight. Under inert atmosphere, a solution of N_3-PEG-OH (0.5 g, 5 kDa, 100 µmol) and DBU (30 µL, 9.29 mmol) in anhydrous DCM (1 mL) was rapidly added to a solution of lactide (2.0 g, 13.9 mmol) in anhydrous DCM (10 mL) and stirred for 8 min at room temperature. The reaction mixture was quenched with an acetic acid solution, precipitated in a

mixture of ethyl ether : hexane (1:1), centrifuged and dried under vacuum overnight. NMR spectroscopic data, Mn and Dispersity were in agreement with those previously described.

Synthesis of DBCO-CpG intermediate

DBCO-PEG-NHS ester (3.78 mg, 5.8 μmol) was dissolved in DMSO (40 μL). The solution was diluted with PBS 1X to reach a final concentration of 10 mM. NH_2-CpG (0.58 μmol) was then reacted with DBCO-PEG4-NHS ester solution for 4 h at room temperature. The solution was purified by size-exclusion chromatography in PBS 1X using a Sephadex G-25 Superfine (mini Quick Spin Oligo) column and stored at -20 °C.

NPs synthesis and conjugation

PEG-*b*-PLA NPs were prepared as previously described [44, 58]. A 1 mL solution of PEG-*b*-PLA and N_3-PEG-*b*-PLA in 75:25 ACN:DMSO (50 mg/mL) was added dropwise to 10 mL of Milli-Q water stirring at 600 rpm. The particles solution was purified in centrifugal filters (Amicon Ultra, MWCO 10 kDa) at 4500 RCF for 1 h and resuspended in PBS to reach a final concentration of 200 mg/mL. DBCO-CpG-C (3 eq) and N_3-PEG-*b*-PLA NPs (1 eq) were reacted *via* copper-free click chemistry in PBS 1X for 12 h at room temperature. After reaction completion, CpG conjugated NPs were purified by size-exclusion chromatography on a Sepharose CL-6B matrix eluting with PBS 1X. Successful purification of the CpG-NPs from unreacted free CpG was confirmed *via* aqueous SEC measurements and agarose gel electrophoresis (4%). The CpG concentration on the NPs was determined through absorption calibration curves at 280 nm acquired using a Synergy H1 Microplate Reader (BioTek Instruments). An individual calibration curve for each NPs valency and TLR9 agonist class was recorded. Conversions between 88 and 97% were measured.

HPMC-C_{12} synthesis

HPMC-C_{12} was prepared according to a previously reported procedure[52]. HPMC (1.0 g) was dissolved in anhydrous NMP by stirring at 80 °C for 1 h. Once cooled to room temperature, 1-dodexylisocyanate (105 mg, 0.5 mmol) and Hunig's base, acting as the catalyst (~ 3 drops) were dissolved in 0.5 mL of anhydrous NMP. This solution was then added dropwise to the reaction mixture, which was stirred at room temperature for 16 h. The polymer was precipitated using acetone, redissolved in Milli-Q water (~ 2 wt%) and dialyzed (3 KDa mesh) against water for 4 days. The polymer mixture was then lyophilized and reconstituted to a 60 mg/mL solution in sterile PBS 1X.

DMF-SEC Measurements

Apparent molecular weight and dispersity were obtained after passing through two size exclusion chromatography columns (Resolve Mixed Bed Low DVB, inner diameter ID of 7.8 mm, M_w range: 200–600,000 g/mol, Jordi Labs) in a mobile phase of *N,N*-dimethylformamide (DMF) with 10 mM LiBr at 35 °C and a flow rate of 1.0 mL/min (Dionex Ultimate 3000 pump, degasser, and autosampler, Thermo Fisher Scientific). Before injection, samples at a concentration of 5 mg/mL were filtered through a 0.22 µm nylon membrane.

Aqueous-SEC Measurements

SEC traces were determined after passing through a size-exclusion chromatography column [5000 to 5,000,000 g/mol]; Superose 6 Increase 10/300 GL (GE Healthcare) in a mobile phase of PBS containing 300 parts per million of sodium azide and at a flow rate of 0.75 mL/min (Dionex Ultimate 3000 pump, degasser, and autosampler, Thermo Fisher Scientific). Detection consisted of an Optilab T-rEX (Wyatt Technology Corporation) refractive index detector operating at 658 nm and a diode array detector operating at 280 nm (Dionex Ultimate 3000, Thermo Fischer Scientific). Before injection, samples at a concentration of 1 mg/mL were filtered through a 0.22 µm PVDF membrane.

Dynamic light scattering and zeta potential

The hydrodynamic diameter and surface charge of the NPs were respectively measured on a DynaPro II plate reader (Wyatt Technology) and a Zetasizer Nano Zs (Malvern Instruments). Three independent measurements were performed for each sample.

PNP and CpG NP Hydrogel formation

CpG polymer-nanoparticle (CpG NP) hydrogels were formed at 2 wt% HPMC-C_{12} and 10 wt% mixture of PEG-*b*-PLA and CpG-PEG-*b*-PLA NPs in PBS. Hydrogels were prepared by mixing a 3:2:1 weight ratio of 6 wt% HPMC-C12 polymer solution, 20 wt% NPs solution, and PBS. Based on the desired adjuvant dosing, 30% CpG conjugated NPs were mixed with non-conjugated PEG-*b*-PLA NPs prior to hydrogel formation. The gels were formed by mixing the solutions using syringes connected through an elbow mixer.

Rheological Characterization of PNP gels

Rheological characterization was completed on a Discovery HR-2 Rheometer (TA Instruments). Measurements were performed using a 20 mm serrated plate geometry at 25 °C and at 500 μm gap height. Dynamic oscillatory frequency sweeps were conducted at a constant 1% strain and angular frequencies from 0.1 to 100 rad/s. Amplitude sweeps were performed at a constant angular frequency of 10 rad/s from 0.5% to 10,000% strain. Flow sweep, steady shear experiments were performed at shear rates from 50 to 0.005 1/s, whereas stress-controlled flow sweep measurements were conducted at shear rates from 0.001 to 10 1/s. Step-shear experiments were performed by alternating between low shear rates (0.1 rad/s for 60 s) and high shear rates (10 rad/s for 30 s) for three full cycles. Yield stress values were extrapolated from stress-controlled flow sweep and amplitude sweep measurements.

FRAP Analysis

Fluorescence recovery after photobleaching (FRAP) was performed on PNP hydrogel and CpG NP hydrogel formulations using a confocal LSM780 microscope. Each individual component of the hydrogel was labelled with a fluorescent dye and analyzed in separate samples. NP-tethered AF647 (10 wt%),

rhodamine-conjugated HPMC-C_{12} (2 wt%), and His-tagged SARS-CoV-2 spike conjugated with HIS-Lite-Cy3 Bis NTA-Ni Complex (0.27 mg per mL of hydrogel) were used to visualize diffusion of the vaccine cargo and gel components. Samples were imaged using low intensity lasers to collect an initial level of fluorescence. Then a high intensity laser with a diameter of 25 µm was focused on the region of interest (ROI) for 10 s to bleach a circular area.

Subsequently, fluorescence emission data was recorded for 4 min to create an exponential fluorescence recovery curve. For each sample, replicate measurements (n = 2-5) were taken at multiple locations. The diffusion coefficient D was calculated according to the following equation[75]:

$$D = \gamma_D \frac{\omega^2}{4\,\tau_{1/2}} \tag{1}$$

where the constant $\gamma_D = \tau_{1/2}/\tau_D$, with $\tau_{1/2}$ being the time to half recovery, τ_D the characteristic diffusion time, both yielded by the ZEN software, and ω the radius of the bleached ROI. The diffusivity of the SARS-CoV-2 spike protein antigen in PBS was calculated using the Stokes-Einstein law equation for diffusion[65]:

$$D = \frac{k_B T}{6\pi\eta R_H} \tag{2}$$

with k_B being the Boltzmann's constant, T the temperature in Kelvin, η the solvent viscosity, and R_H the solute hydrodynamic radius. The hydrodynamic radius of the spike protein was measured via DLS to be R_H = 12.2 nm, whereas η for PBS was approximated to be 0.8872 mPa s at 25 °C. The measured R_H agrees with the value published in literature and measured via Cryo-EM[76].

Vaccine formulation

SARS-CoV-2 spike protein vaccines were injected subcutaneously either in form of a soluble injection or in form of a gel. For soluble injections, vaccine formulations contained a 10 µg antigen dose of spike S1+S2 ECD (R683A, R685A, F817P, A892P, A899P, A942P, K986P, V987P)-His Recombinant Protein (Sino Biological 40589-V08H4) and a 20 µg 30% CpG NPs adjuvant dose; boosting was performed on day 21. For the CpG NP hydrogels, the dose was doubled and contained 20 µg of antigen and 40 µg of CpG

NPs adjuvant; for the gel group, boosting was not performed. Control groups were composed of non-conjugated PEG-*b*-PLA NPs and soluble CpG (20 µg, IDT) vaccines. Mouse blood was collected from the tail vein each week for 10 weeks. To analyze early cytokine response, blood was collected at 0 h, at 3 h and 24 h from injection and stored at -80 °C. The serum samples were analyzed for IFN-α and TNF-α levels and the concentrations were determined via enzyme-linked immunosorbent assay (ELISA) according to manufacturer's instructions and were calculated from standard curves. Absorbance was measured with a Synergy H1 microplate reader (BioTek Instruments) at 450 nm.

In vitro Raw-Blue reporter assay

The Raw-Blue (NF-kB-SEAP) reporter cell line (Invivogen, raw-sp) was used to evaluate the valency effect of TLR9 agonist conjugated to PEG-*b*-PLA NPs. The cells were cultured at 37 °C with 5% CO_2 in DMEM supplemented with L-glutamine (2 mM), D-glucose (4.5 g/L), 10% HI-FBS, and penicillin (100 U/mL)/streptomycin (100 µg). Every other passage, zeocin (100 µg/mL) was added to the culture medium. Serial dilutions of soluble CpG and of the different CpG NPs formulations were added to a 96-well tissue culture treated plate to achieve final concentrations between 30 and 3.1 µg/mL of TLR9 agonist. Non-conjugated PEG-*b*-PLA NPs was used as a negative control. About 100,000 cells were added to each well in 180 µL of media and were incubated for 21 h at 37 °C in a CO_2 (5%) incubator. Manufacturer instructions were followed for SEAP quantification, and absorbance levels detected at 655 nm after 3 h incubation with QUANTI-Blue Solution (Invivogen). Nonlinear regression fits were found using the "Log(agonist) vs. response – EC_{50}" function in GraphPad Prism 8.4 software.

Animal studies

Six-to-seven weeks old female C57BL/6 (B6) mice were obtained from Charles River, housed in the animal facility at Stanford University and cared for according to Institutional Animal Care and Use guidelines. All animal studies were performed in accordance with the National Institutes of Health guidelines and the approval of Stanford Administrative Panel on Laboratory Animal Care. The day before

vaccine administration, mice were shaved in order to receive a subcutaneous injection of 150 µL of CpG NP hydrogel or 100 µL of soluble vaccine on the right side of their backs. Mouse blood was collected from the tail veins each week for 10 weeks.

Mouse Serum ELISAs

Serum Anti-spike IgG antibody endpoint titers were measured using an ELISA. Maxisorp plates (Thermofisher) were coated with SARS-CoV-2 spike protein (Sino Biological 40591-V08H4), the mutant spike from Beta B.1.351 (Sino Biological 40591-V08H12), the mutant spike from Delta B.1.617.2 (Sino Biological 40591-V08H23), or the mutant spike from Omicron B.1.1.529 (Sino Biological 40591-V08H41) at 2 µg/mL in PBS overnight at 4 °C and subsequently blocked with PBS containing 1 wt% BSA for 1 h at 25 °C. Serum samples were serially diluted and incubated in the previously coated plates for 2 h at 25 °C, and goat-anti-mouse IgG Fc-HRP (1:10,000), IgG1 Fc-HRP (1:10,000), or IgG2c (1:10,000) was added for 1h at 25 °C. Plates were developed with TMB substrate, the reaction stopped with 1 M HCl and the plates analyzed using a Synergy H1 microplate reader (BioTek Instruments) at 450 nm. End point titers were defined as the highest serum dilution at the one an optical density above 0.1 was detected.

SARS-CoV-2 Spike-pseudotyped Viral Neutralization Assay

Neutralization assays were conducted as previously described.[77] Briefly, SARS-CoV-2 spike pseudotyped lentivirus was produced in HEK239T cells and cells seeded at six million cells the day prior to transfection. A five-plasmid system was used for viral production. Plasmids were added to filter-sterilized water and HEPES-buffered saline was added dropwise to reach a final volume of 1 mL. To form transfection complexes, $CaCl_2$ was added dropwise to the gently agitated solution. The transfection reactions were incubated for 20 min at RT and then added to plated cells. Virus-containing culture supernatants were harvested ~72 hours after transfection via centrifugation and filtered through a 0.45 µm syringe filter. Viral stocks were stored at -80 °C. For the neutralization assays, ACE2/HeLa cells were plated 1 to 2 days prior to infection and mouse serum was heat inactivated at 56 °C for 30 min prior to use.

Mouse serum (1:50 dilution) and virus were diluted in cell culture medium and supplemented with polybrene at a final concentration of 5 µg/mL. Serum/virus solution at 1:50 were incubated at 37 °C for 1 h. After the 1 h incubation, the media was removed from the cells and incubated with the serum/virus solution at 37°C for 48 h. After complete incubation, the cells were then lysed using BriteLite (Perkin Elmer) luciferase readout reagent, and luminescence was measured with a BioTek plate reader. Each plate was normalized by averaging the readout from the wells containing only the virus or only the cells.

Statistical Analysis

All results are expressed as mean ± standard deviation (*s.d*). Comparison between two groups were conducted by a two-tailed Student's t-test. One-way ANOVA tests with a Tukey's multiple-comparisons test was used for comparison across multiple groups. For plots displaying multiple time points or protection against different variants, P values were determined with a 2way ANOVA with Tukey's multiple-comparisons test. Statistical analysis was performed using GraphPad Prism 8.4 (GraphPad Software). Statistical significance was considered as $p < 0.05$.

FIGURES

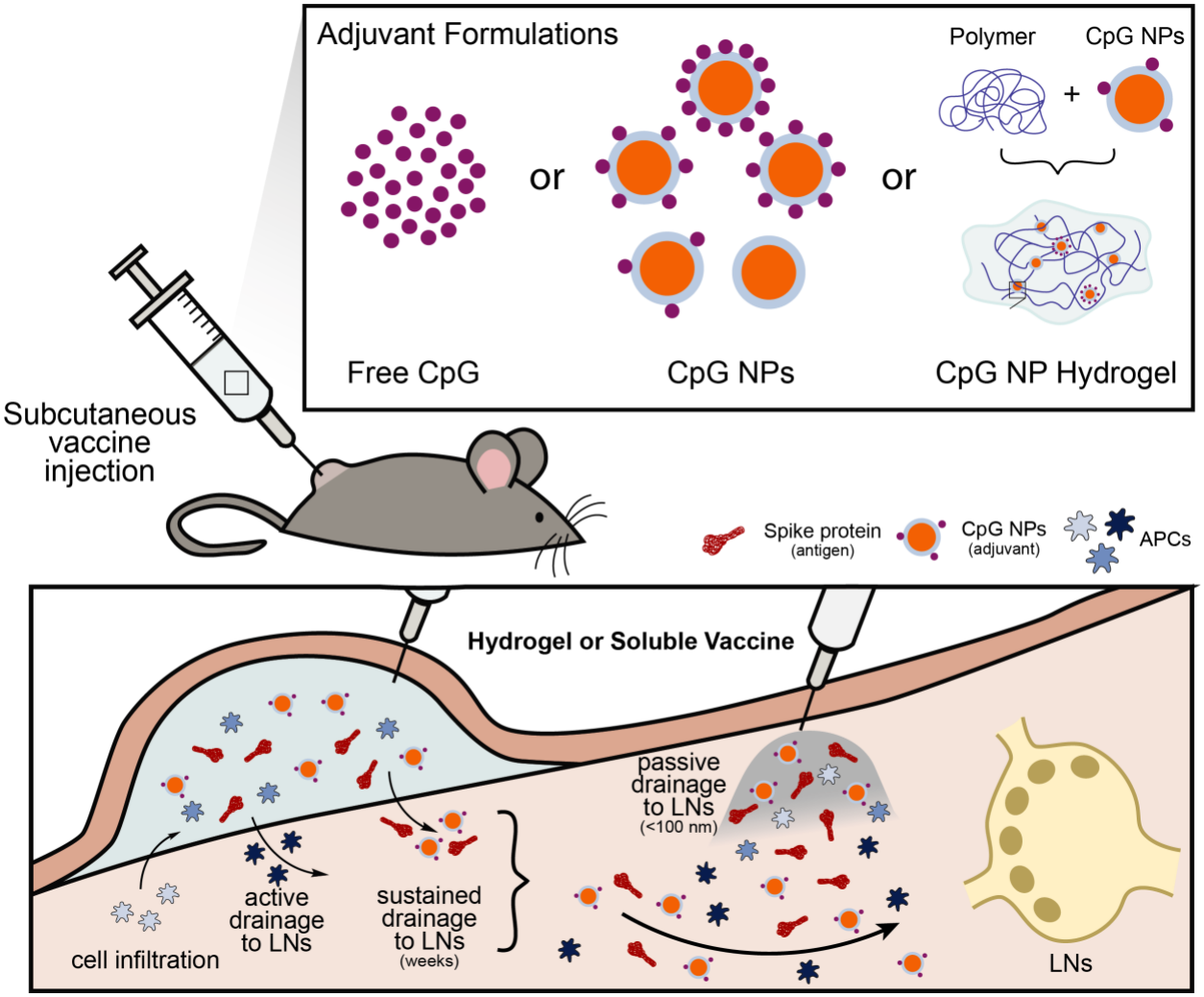

Figure 1: Schematic representation of a subcutaneous vaccine injection in a mouse model for in vivo release. Delivery of CpG adjuvant can be achieved in different ways: as a free species, tethered to PEG-b-PLA NPs or tethered to NPs and encapsulated in polymer-nanoparticle (PNP) hydrogels. PNP hydrogels are loaded with vaccine cargo, including antigen and adjuvant (CpG NPs), and allow for sustained vaccine exposure. After subcutaneous injection of the hydrogel vaccine, vaccine components can be transported to the lymph nodes (LNs) either by drainage through antigen presenting cells (APCs) that have previously infiltrated the gel, or by LN drainage of the single vaccine components themselves. Soluble vaccines, on the other hand, do not create an inflammatory niche for cell infiltration. Vaccine components are rapidly cleared from the body and drained to the lymph nodes, potentially decreasing the potency. Nanoparticle vaccine cargos, such as CpG NPs, however, may improve immune cells activation and LN targeting ability.

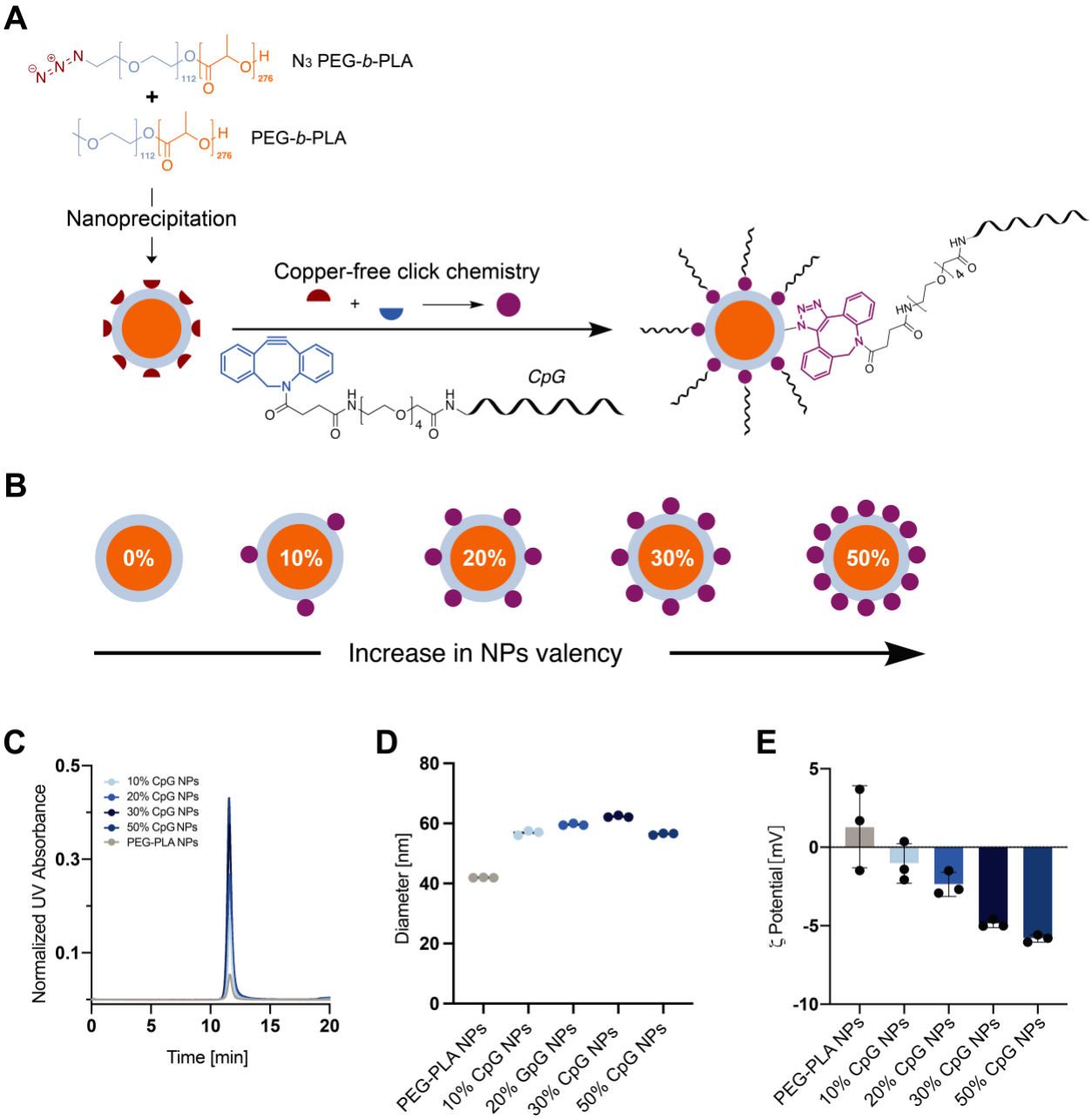

Figure 2: Design of CpG functionalized NPs. (A) Synthetic scheme for the fabrication of CpG-based NPs. Formation of azide-terminated PEG-b-PLA NPs via nanoprecipitation followed by copper-free click chemistry with DBCO-CpG to yield to CpG-functionalized NPs. 10%, 20%, 30% and 50% valencies were achieved by mixing different ratios of PEG-b-PLA and N_3-PEG-b-PLA polymer solutions before nanoprecipitation. **(B)** Normalized UV absorbance of 10%, 20%, 30% and 50% CpG-functionalized NPs. **(C)** Hydrodynamic diameters of PEG-b-PLA NPs and CpG NPs in PBS. **(D)** Surface zeta potential of PEG-b-PLA NPs and CpG NPs in PBS. P values listed were determined using a 1way ANOVA with Tukey's multiple comparisons test. P values for comparisons between the PEG-b-PLA NPs group and all other groups are shown above the points; *: $p < 0.05$, **: $p < 0.01$, ***: $p < 0.001$, ****: $p < 0.0001$, ns: not significant.

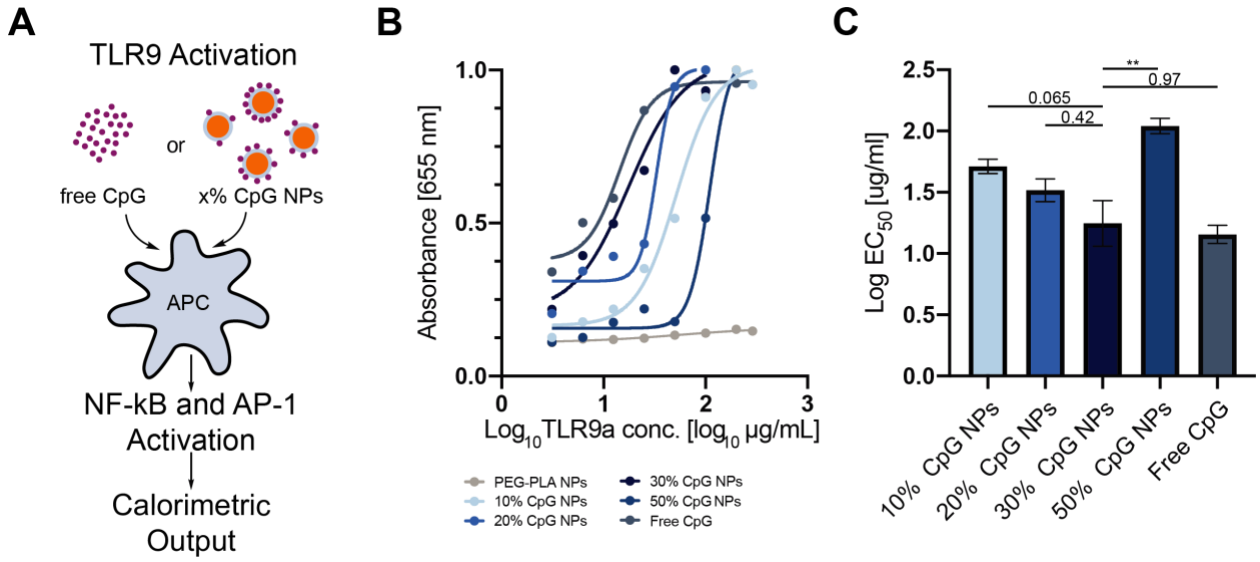

Figure 3: In vitro activity of CpG functionalized NPs. (A) Incubation of Raw-Blue macrophage cells (APCs) with either free CpG or different valencies of CpG NPs (10%, 20%, 30%, 50%) induces the activation of NF-kB and AP-1. The magnitude of activation is quantified via calorimetric output using QUANTI-Blue solution. **(B)** Activation curves across a range of CpG concentrations (3.1–29 µg/mL) delivered on CpG NPs at different densities to 100,000 Raw-Blue cells. The absorbance at 655 nm corresponds to TLR activation. **(C)** Log EC_{50} values for each activation curve were extrapolated from **(B)** using a "log(TLR9 agonist) vs response" nonlinear regression curve fit of the dilution curves. P values listed were determined using a 1way ANOVA with Tukey's multiple comparisons test. P values for comparisons between the 30% CpG NPs group and all other groups are shown above the points: *: $p < 0.05$, **: $p < 0.01$, ***: $p < 0.001$, ****: $p < 0.0001$, ns: not significant.

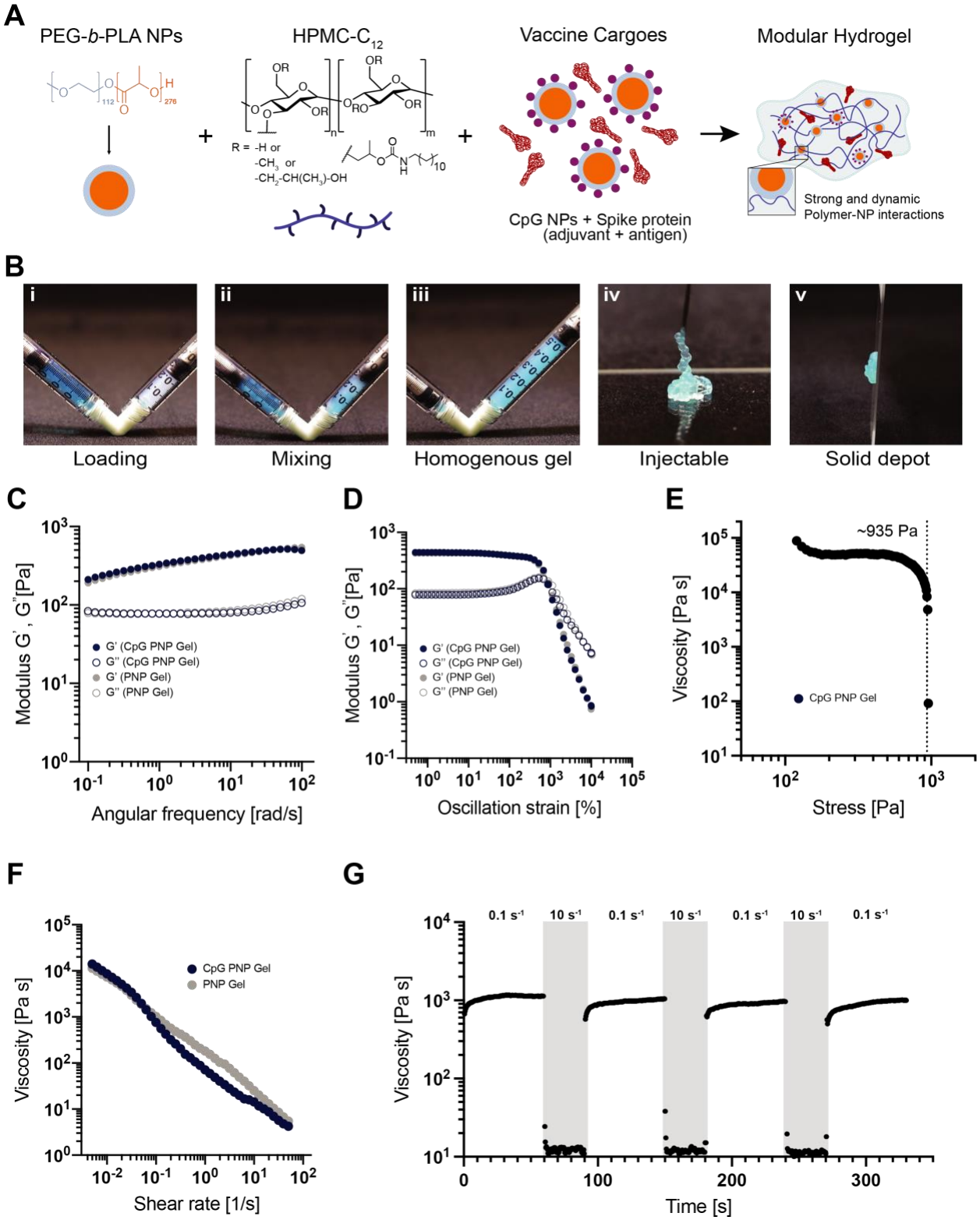

Figure 4: Fabrication and characterization of CpG - Polymer-Nanoparticle (PNP) hydrogels. (A) Vaccine loaded CpG NP hydrogels are formed when aqueous solutions of PEG-b-PLA NPs and dodecyl-modified hydroxypropylmethylcellulose (HPMC-C_{12}) are mixed together with aqueous solutions of vaccine cargo comprising CpG NPs (adjuvant) and spike protein (antigen). **(B)** Vaccine cargo are added to the

aqueous NPs solution before loading the aqueous and polymer components in two separate syringes (i), mixing the two phases with an elbow mixer (ii) leads to homogeneous hydrogels (iii). Image of a PNP hydrogel flowing through a 21-gauge needle during injection (iv) and formation of solid-like depot after injection (v). **(C)** Frequency-dependent oscillatory shear rheology and oscillatory amplitude sweeps **(D)** of CpG NP and unloaded PNP hydrogels. **(E)** Stress-controlled flow sweeps of the CpG NP gel and yield stress value. **(F)** Shear-dependent viscosities of the two analyzed hydrogels demonstrate shear thinning and yielding effects, decreasing with increased shear rate. **(G)** Step-shear measurements over 3 cycles model yielding and healing of the hydrogels. Alternating low shear rates (0.1 1/s), and high shear rates (10.0 1/s, gray color) are imposed for 60 and 30 s respectively.

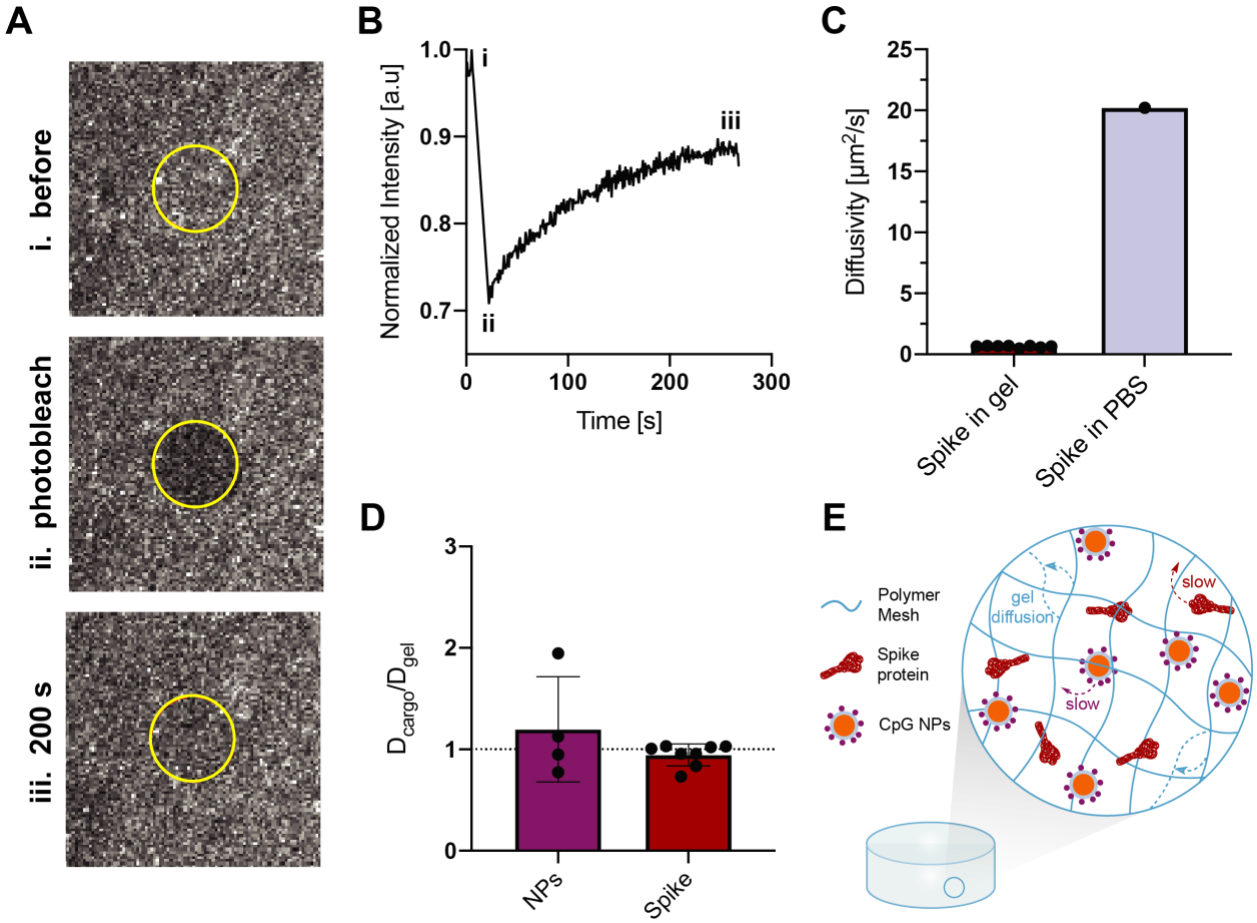

Figure 5: Diffusivity of the cargo and gel components in the CpG-NP hydrogel. (A) FRAP microscopy images of the selected area to be photobleached (i) before bleaching, (ii) right after the bleaching process and (iii) after complete fluorescence recovery. **(B)** Representative fluorescence recovery curve over time of the spike protein at a concentration of 0.27 mg per mL of gel. Timepoints representing (A) are outlined on the curve. **(C)** Diffusivities of spike protein in PNP (n = 8) hydrogels measured via FRAP and diffusivity of spike in PBS calculated using Stokes-Einstein equation (Eq. (2)). **(D)** NPs and spike protein diffusivities in the hydrogel are measured via FRAP and are represented normalized by Dgel, the polymer matrix diffusivity. Values close to 1 represent diffusivities similar to the polymer matrix and support the assumption that NPs and spike antigen are caught in the hydrogel network. The dotted line shows Dcargo/Dgel = 1 (n = 4-8). **(E)** Representative schematic of the vaccine loaded PNP hydrogel, showing all the components diffuse slowly within the hydrogel network. All the results are given as mean ± s.d.

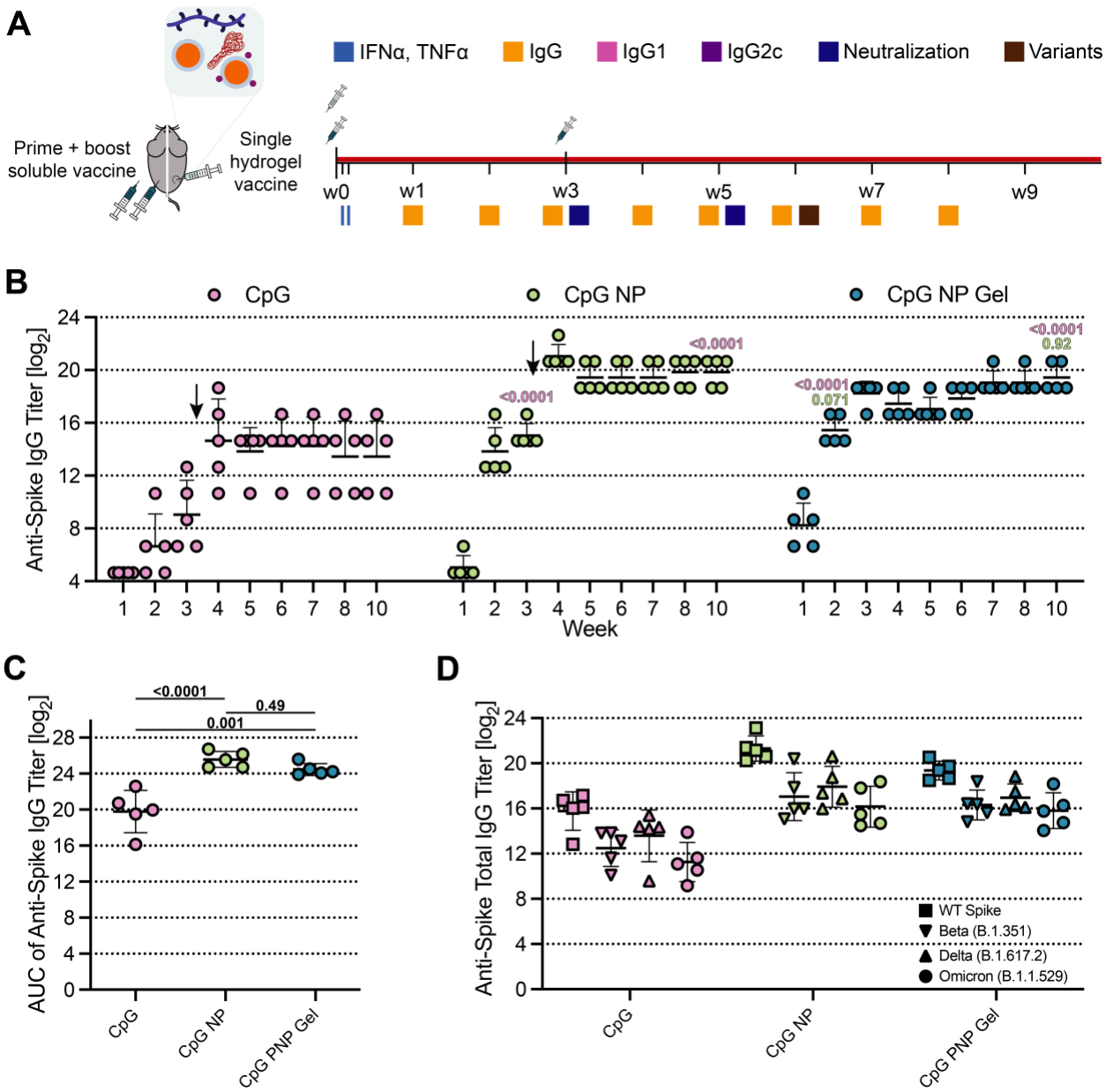

Figure 6: In vivo humoral response to COVID-19 subunit vaccine. (A) Timeline of mouse immunizations and blood collection for different assays. Soluble vaccine groups were immunized with a prime dose of 10 µg spike antigen and 20 µg CpG NPs or soluble CpG at day 0 and received a booster injection of the same treatment at day 21. CpG NP hydrogel group was immunized with a single dose of 20 µg of spike antigen and 40 µg of CpG NP adjuvant at day 0. Serum was collected over time to determine cytokine levels and IgG titers. IgG1, IgG2b, and IgG2c titers were quantified and neutralization assays were conducted on day 21 and day 35 serum. **(B)** Anti-spike total IgG ELISA endpoint titer of soluble vaccines before and after boosting (arrow) and single immunization CpG NP hydrogel. **(C)** Area under the curve (AUC) of anti-spike titers from (B). **(D)** Anti-spike IgG ELISA titers from serum collected on week 6, 3 weeks after boosting the soluble vaccine groups.Titers were determined for wildtype spike as well as Beta (B.1.351), Delta (B.1.617.2, and Omicron (B.1.1.529) variants of the spike protein. Each point represents an individual mouse (n = 5). Data are shown as mean +/- s.d. P values listed were determined using a 1way or 2way ANOVA with Tukey's multiple comparisons test on the logged titer values for IgG titer comparisons (including total IgG and spike variants). P values for comparisons are shown above the points.

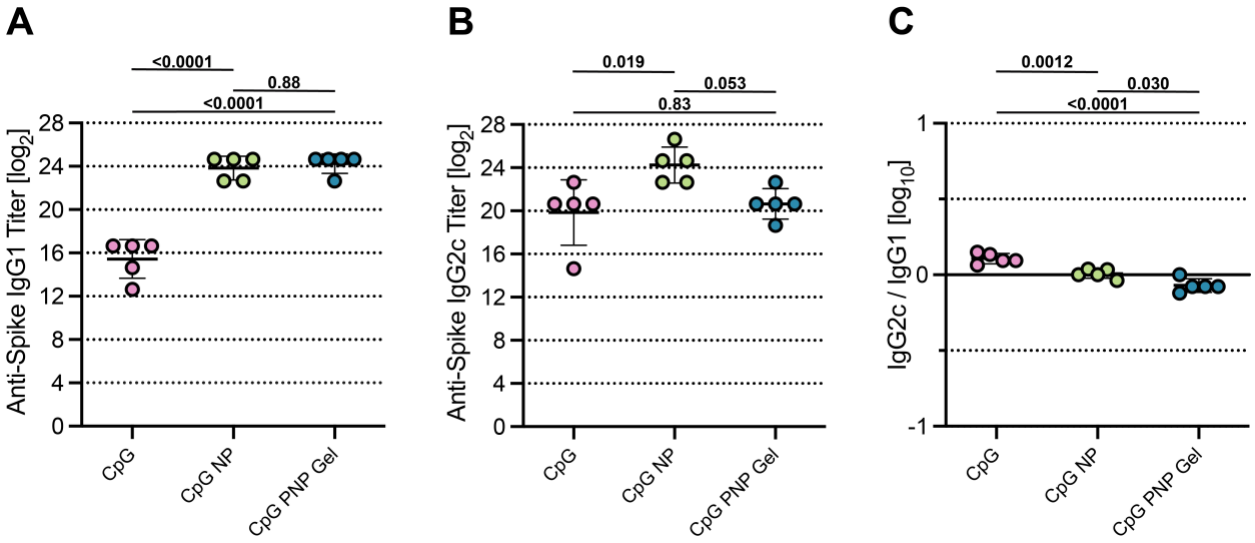

Figure 7: Antibody subtype response to COVID-19 subunit vaccine. Anti-spike IgG1 **(A)** and IgG2c **(B)** titers from serum collected on week 5, 2 weeks after boosting the soluble vaccine groups. **(C)** The ratio of Anti-spike IgG2c to IgG1 post-boost titers. Lower values (below 1) suggest a Th2 response or humoral response, and higher values (above 1) suggest a Th1 response or cellular response. Each point represents an individual mouse (n = 5). Data are shown as mean +/- s.d. P values listed were determined using a 1way or ANOVA with Tukey's multiple comparisons test on the logged titer values for IgG titer comparisons. P values for comparisons are shown above the points.

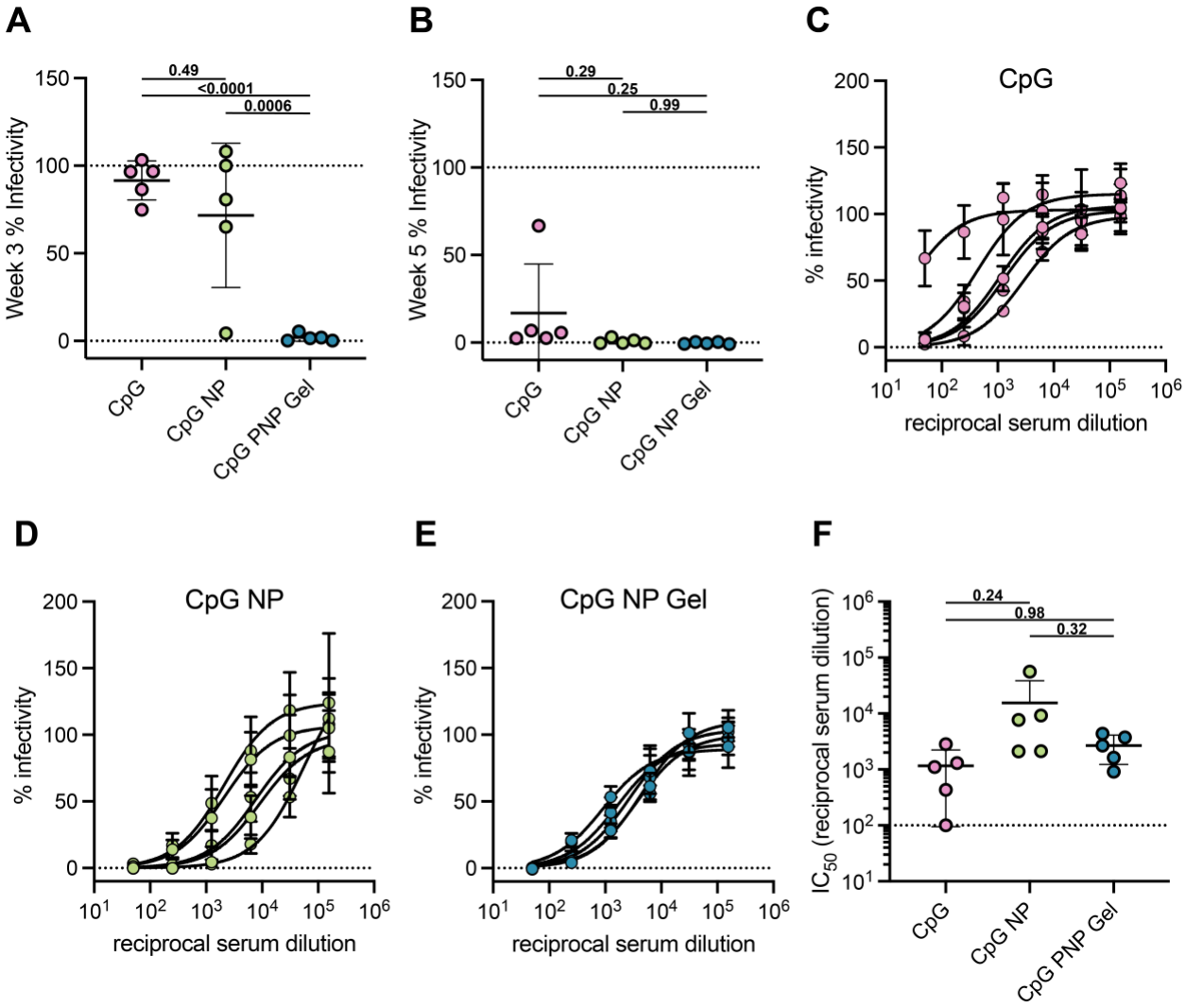

Figure 8: Single immunization of CpG NP hydrogel elicits neutralizing antibodies in mice. (A) Pre-boost (Day 21) spike-pseudotyped viral neutralization assays for the CpG-adjuvanted COVID-19 spike vaccines at a serum dilution of 1:50. **(B)** Post-boost for soluble vaccines (Day 35) spike-pseudotyped viral neutralization assays for the CpG-adjuvanted COVID-19 spike vaccines at a serum dilution of 1:50. **(C-E)** Percent infectivity for all treatment groups at a range of Week 5 serum dilutions as determined by a SARS-CoV-2 spike-pseudotyped viral neutralization assay. **(F)** Comparison of IC_{50} values determined from neutralization curves on Day 35 for soluble vaccine formulations (prime-boosted) and hydrogel vaccine (single immunization) following immunization with CpG-adjuvanted COVID-19 spike vaccines. Each point represents an individual mouse (n = 5). Data are shown as mean +/- s.d. P values listed were determined using a 1way ANOVA with Tukey's multiple comparisons. P values for comparisons are shown above the points.

ASSOCIATED CONTENT

Supporting Information.

The following files are available free of charge.

Additional tables and figures of synthesis, purification, and characterization of CpG NPs, and additional immune response data and figures. (PDF)

AUTHOR INFORMATION

Corresponding Author

Eric A. Appel

Department of Materials Science & Engineering, Department of Bioengineering, Stanford ChEM-H Institute, Department of Pediatrics – Endocrinology, and Woods Institute for the Environment, Stanford University, Stanford CA 94305, USA

E: eappel@stanford.edu

Author Contributions

BSO, VTM, ECG and EAA designed the broad concepts and research studies. JB, AEP, OMS, and HLP designed specific experiments. BSO, VTM, JB, ECG, AEP, OMS, JY, and HLP performed research and experiments. BSO, VTM, and EAA wrote the paper. BSO, JB, OSM, and JY edited the paper. The manuscript was written through contributions of all authors. All authors have given approval to the final version of the manuscript. ‡These authors contributed equally.

Conflict of Interest Statement

E.A.A, V.C.T.M.P, and E.C.G. are listed as inventors on a pending patent application. All other authors declare no conflicts of interest.

ACKNOWLEDGMENTS

We would like to thank all members of the Appel lab for their useful discussion and advice throughout this project. Also, the staff of the BioE/ChemE Animal Facility who cared for our mice. This work was financially supported by the Center for Human Systems Immunology with the Bill & Melinda Gates Foundation (OPP1113682; OPP1211043; INV027411), the American Cancer Society (RSG-18-133-01-CDD), the Goldman Sachs Foundation (administered by the Stanford Cancer Institute, SPO# 162509), and a Bio-X Interdisciplinary Initiatives Seed Grant. BSO is grateful for an Eastman Kodak Fellowship. JB is thankful for a Marie-Curie fellowship from the European Union (H2020; No. 101030481). OMS and JY are thankful for a National Science Foundation Graduate Research Fellowship. This work was also supported by the Stanford Maternal and Child Health Research Institute postdoctoral fellowship (to AEP). We thank Dr. Jesse Bloom, Kate Crawford, Dr. Dennis Burton, and Dr. Deli Huang for sharing the plasmids, cells, and invaluable advice for implementation of the spike-pseudotyped lentiviral neutralization assay (to AEP). We also thank Dr. Peter S. Kim for his advice and support.

REFERENCES

1. WHO Global Vaccine Action Plan 2011-2020. https://www.who.int/publications/i/item/global-vaccine-action-plan-2011-2020.
2. WHO Coronavirus (COVID-19) Dashboard. https://covid19.who.int/.
3. Vartak, A.; Sucheck, S. J., Recent Advances in Subunit Vaccine Carriers. *Vaccines (Basel)* **2016,** *4* (2).
4. Reed, S. G.; Orr, M. T.; Fox, C. B., Key roles of adjuvants in modern vaccines. *Nat Med* **2013,** *19* (12), 1597-608.
5. Coffman, R. L.; Sher, A.; Seder, R. A., Vaccine adjuvants: putting innate immunity to work. *Immunity* **2010,** *33* (4), 492-503.
6. Campbell, J. D., Development of the CpG Adjuvant 1018: A Case Study. *Methods Mol Biol* **2017,** *1494*, 15-27.
7. Ballester, M.; Nembrini, C.; Dhar, N.; de Titta, A.; de Piano, C.; Pasquier, M.; Simeoni, E.; van der Vlies, A. J.; McKinney, J. D.; Hubbell, J. A.; Swartz, M. A., Nanoparticle conjugation and pulmonary delivery enhance the protective efficacy of Ag85B and CpG against tuberculosis. *Vaccine* **2011,** *29* (40), 6959-66.
8. Krieg, A. M., CpG still rocks! Update on an accidental drug. *Nucleic Acid Ther* **2012,** *22* (2), 77-89.
9. Sen, D.; Forrest, L.; Kepler, T. B.; Parker, I.; Cahalan, M. D., Selective and site-specific mobilization of dermal dendritic cells and Langerhans cells by Th1- and Th2-polarizing adjuvants. *Proc Natl Acad Sci U S A* **2010,** *107* (18), 8334-9.
10. Kuai, R.; Ochyl, L. J.; Bahjat, K. S.; Schwendeman, A.; Moon, J. J., Designer vaccine nanodiscs for personalized cancer immunotherapy. *Nat Mater* **2017,** *16* (4), 489-496.
11. Ballester, M.; Jeanbart, L.; de Titta, A.; Nembrini, C.; Marsland, B. J.; Hubbell, J. A.; Swartz, M. A., Nanoparticle conjugation enhances the immunomodulatory effects of intranasally delivered CpG in house dust mite-allergic mice. *Sci Rep* **2015,** *5*, 14274.
12. Kuo, T.-Y.; Lin, M.-Y.; Coffman, R. L.; Campbell, J. D.; Traquina, P.; Lin, Y.-J.; Liu, L. T.-C.; Cheng, J.; Wu, Y.-C.; Wu, C.-C.; Tang, W.-H.; Huang, C.-G.; Tsao, K.-C.; Chen, C., Development of CpG-adjuvanted stable prefusion SARS-CoV-2 spike antigen as a subunit vaccine against COVID-19. *Scientific Reports* **2020,** *10* (1).
13. de Titta, A.; Ballester, M.; Julier, Z.; Nembrini, C.; Jeanbart, L.; van der Vlies, A. J.; Swartz, M. A.; Hubbell, J. A., Nanoparticle conjugation of CpG enhances adjuvancy for cellular immunity and memory recall at low dose. *Proc Natl Acad Sci U S A* **2013,** *110* (49), 19902-7.
14. Buss, C. G.; Bhatia, S. N., Nanoparticle delivery of immunostimulatory oligonucleotides enhances response to checkpoint inhibitor therapeutics. *Proc Natl Acad Sci U S A* **2020,** *117* (24), 13428-13436.
15. COVID-19 vaccine tracker and landscape. https://www.who.int/publications/m/item/draft-landscape-of-covid-19-candidate-vaccines.
16. Francica, J. R.; Lynn, G. M.; Laga, R.; Joyce, M. G.; Ruckwardt, T. J.; Morabito, K. M.; Chen, M.; Chaudhuri, R.; Zhang, B.; Sastry, M.; Druz, A.; Ko, K.; Choe, M.; Pechar, M.; Georgiev, I. S.; Kueltzo, L. A.; Seymour, L. W.; Mascola, J. R.; Kwong, P. D.; Graham, B. S.; Seder, R. A., Thermoresponsive Polymer Nanoparticles Co-deliver RSV F Trimers with a TLR-7/8 Adjuvant. *Bioconjug. Chem.* **2016,** *27* (10), 2372-2385.
17. Lynn, G. M.; Laga, R.; Darrah, P. A.; Ishizuka, A. S.; Balaci, A. J.; Dulcey, A. E.; Pechar, M.; Pola, R.; Gerner, M. Y.; Yamamoto, A.; Buechler, C. R.; Quinn, K. M.; Smelkinson,

M. G.; Vanek, O.; Cawood, R.; Hills, T.; Vasalatiy, O.; Kastenmuller, K.; Francica, J. R.; Stutts, L.; Tom, J. K.; Ryu, K. A.; Esser-Kahn, A. P.; Etrych, T.; Fisher, K. D.; Seymour, L. W.; Seder, R. A., In vivo characterization of the physicochemical properties of polymer-linked TLR agonists that enhance vaccine immunogenicity. *Nat Biotechnol* **2015,** *33* (11), 1201-10.
18. Irvine, D. J.; Aung, A.; Silva, M., Controlling timing and location in vaccines. *Adv Drug Deliv Rev* **2020**.
19. Gale, E. C.; Roth, G. A.; Smith, A. A. A.; Alcántara-Hernández, M.; Idoyaga, J.; Appel, E. A., A Nanoparticle Platform for Improved Potency, Stability, and Adjuvanticity of Poly(I:C). *Advanced Therapeutics* **2020,** *3* (1), 1900174.
20. Wilson, D. S.; Hirosue, S.; Raczy, M. M.; Bonilla-Ramirez, L.; Jeanbart, L.; Wang, R.; Kwissa, M.; Franetich, J. F.; Broggi, M. A. S.; Diaceri, G.; Quaglia-Thermes, X.; Mazier, D.; Swartz, M. A.; Hubbell, J. A., Antigens reversibly conjugated to a polymeric glyco-adjuvant induce protective humoral and cellular immunity. *Nat Mater* **2019,** *18* (2), 175-185.
21. Kasturi, S. P.; Skountzou, I.; Albrecht, R. A.; Koutsonanos, D.; Hua, T.; Nakaya, H. I.; Ravindran, R.; Stewart, S.; Alam, M.; Kwissa, M.; Villinger, F.; Murthy, N.; Steel, J.; Jacob, J.; Hogan, R. J.; Garcia-Sastre, A.; Compans, R.; Pulendran, B., Programming the magnitude and persistence of antibody responses with innate immunity. *Nature* **2011,** *470* (7335), 543-U136.
22. Nederberg, F.; Appel, E.; Tan, J. P.; Kim, S. H.; Fukushima, K.; Sly, J.; Miller, R. D.; Waymouth, R. M.; Yang, Y. Y.; Hedrick, J. L., Simple approach to stabilized micelles employing miktoarm terpolymers and stereocomplexes with application in paclitaxel delivery. *Biomacromolecules* **2009,** *10* (6), 1460-8.
23. Shi, J.; Xiao, Z.; Kamaly, N.; Farokhzad, O. C., Self-assembled targeted nanoparticles: evolution of technologies and bench to bedside translation. *Acc Chem Res* **2011,** *44* (10), 1123-34.
24. Valencia, P. M.; Hanewich-Hollatz, M. H.; Gao, W.; Karim, F.; Langer, R.; Karnik, R.; Farokhzad, O. C., Effects of ligands with different water solubilities on self-assembly and properties of targeted nanoparticles. *Biomaterials* **2011,** *32* (26), 6226-33.
25. Ghasemi, R.; Abdollahi, M.; Emamgholi Zadeh, E.; Khodabakhshi, K.; Badeli, A.; Bagheri, H.; Hosseinkhani, S., mPEG-PLA and PLA-PEG-PLA nanoparticles as new carriers for delivery of recombinant human Growth Hormone (rhGH). *Sci Rep* **2018,** *8* (1), 9854.
26. Elsabahy, M.; Wooley, K. L., Design of polymeric nanoparticles for biomedical delivery applications. *Chemical Society Reviews* **2012,** *41* (7), 2545-2561.
27. Tan, J. P.; Kim, S. H.; Nederberg, F.; Appel, E. A.; Waymouth, R. M.; Zhang, Y.; Hedrick, J. L.; Yang, Y. Y., Hierarchical supermolecular structures for sustained drug release. *Small* **2009,** *5* (13), 1504-7.
28. Ou, B. S.; Saouaf, O. M.; Baillet, J.; Appel, E. A., Sustained delivery approaches to improving adaptive immune responses. *Advanced Drug Delivery Reviews* **2022,** *187*, 114401.
29. Roth, G. A.; Picece, V. C. T. M.; Ou, B. S.; Luo, W.; Pulendran, B.; Appel, E. A., Designing spatial and temporal control of vaccine responses. *Nature Reviews Materials* **2021**.
30. Reddy, S. T.; Rehor, A.; Schmoekel, H. G.; Hubbell, J. A.; Swartz, M. A., In vivo targeting of dendritic cells in lymph nodes with poly(propylene sulfide) nanoparticles. *J Control Release* **2006,** *112* (1), 26-34.
31. Manolova, V.; Flace, A.; Bauer, M.; Schwarz, K.; Saudan, P.; Bachmann, M. F., Nanoparticles target distinct dendritic cell populations according to their size. *Eur J Immunol* **2008,** *38* (5), 1404-13.

32. Rao, D. A.; Forrest, M. L.; Alani, A. W.; Kwon, G. S.; Robinson, J. R., Biodegradable PLGA based nanoparticles for sustained regional lymphatic drug delivery. *J Pharm Sci* **2010,** *99* (4), 2018-31.
33. Reddy, S. T.; van der Vlies, A. J.; Simeoni, E.; Angeli, V.; Randolph, G. J.; O'Neil, C. P.; Lee, L. K.; Swartz, M. A.; Hubbell, J. A., Exploiting lymphatic transport and complement activation in nanoparticle vaccines. *Nat Biotechnol* **2007,** *25* (10), 1159-64.
34. Jiang, H.; Wang, Q.; Sun, X., Lymph node targeting strategies to improve vaccination efficacy. *J Control Release* **2017,** *267*, 47-56.
35. Schudel, A.; Francis, D. M.; Thomas, S. N., Material design for lymph node drug delivery. *Nature Reviews Materials* **2019,** *4* (6), 415-428.
36. Howard, G. P.; Verma, G.; Ke, X.; Thayer, W. M.; Hamerly, T.; Baxter, V. K.; Lee, J. E.; Dinglasan, R. R.; Mao, H.-Q., Critical size limit of biodegradable nanoparticles for enhanced lymph node trafficking and paracortex penetration. *Nano Research* **2019,** *12* (4), 837-844.
37. Merad, M.; Sathe, P.; Helft, J.; Miller, J.; Mortha, A., The dendritic cell lineage: ontogeny and function of dendritic cells and their subsets in the steady state and the inflamed setting. *Annu Rev Immunol* **2013,** *31*, 563-604.
38. Kato, Y.; Abbott, R. K.; Freeman, B. L.; Haupt, S.; Groschel, B.; Silva, M.; Menis, S.; Irvine, D. J.; Schief, W. R.; Crotty, S., Multifaceted Effects of Antigen Valency on B Cell Response Composition and Differentiation In Vivo. *Immunity* **2020,** *53* (3), 548-563 e8.
39. Gale, E. C.; Roth, G. A.; Smith, A. A.; Alcántara-Hernández, M.; Idoyaga, J.; Appel, E. A., A Nanoparticle Platform for Improved Potency, Stability, and Adjuvanticity of Poly (I: C). *Advanced Therapeutics* **2020,** *3* (1), 1900174.
40. Tang, S.; Liu, Z.; Xu, W.; Li, Q.; Han, T.; Pan, D.; Yue, N.; Wu, M.; Liu, Q.; Yuan, W.; Huang, Z.; Zhou, D.; Zhou, W.; Qian, Z., Versatile Functionalization of Ferritin Nanoparticles by Intein-Mediated Trans-Splicing for Antigen/Adjuvant Co-delivery. *Nano Lett* **2019,** *19* (8), 5469-5475.
41. Tsai, S. J.; Black, S. K.; Jewell, C. M., Leveraging the Modularity of Biomaterial Carriers to Tune Immune Responses. *Advanced Functional Materials* **2020,** *n/a* (n/a), 2004119.
42. Irvine, D. J.; Swartz, M. A.; Szeto, G. L., Engineering synthetic vaccines using cues from natural immunity. *Nat Mater* **2013,** *12* (11), 978-90.
43. Demuth, P. C.; Garcia-Beltran, W. F.; Ai-Ling, M. L.; Hammond, P. T.; Irvine, D. J., Composite dissolving microneedles for coordinated control of antigen and adjuvant delivery kinetics in transcutaneous vaccination. *Adv Funct Mater* **2013,** *23* (2), 161-172.
44. Roth, G. A.; Gale, E. C.; Alcantara-Hernandez, M.; Luo, W.; Axpe, E.; Verma, R.; Yin, Q.; Yu, A. C.; Lopez Hernandez, H.; Maikawa, C. L.; Smith, A. A. A.; Davis, M. M.; Pulendran, B.; Idoyaga, J.; Appel, E. A., Injectable Hydrogels for Sustained Codelivery of Subunit Vaccines Enhance Humoral Immunity. *ACS Cent Sci* **2020,** *6* (10), 1800-1812.
45. Tam, H. H.; Melo, M. B.; Kang, M.; Pelet, J. M.; Ruda, V. M.; Foley, M. H.; Hu, J. K.; Kumari, S.; Crampton, J.; Baldeon, A. D.; Sanders, R. W.; Moore, J. P.; Crotty, S.; Langer, R.; Anderson, D. G.; Chakraborty, A. K.; Irvine, D. J., Sustained antigen availability during germinal center initiation enhances antibody responses to vaccination. *Proc Natl Acad Sci U S A* **2016,** *113* (43), E6639-E6648.
46. Boopathy, A. V.; Mandal, A.; Kulp, D. W.; Menis, S.; Bennett, N. R.; Watkins, H. C.; Wang, W.; Martin, J. T.; Thai, N. T.; He, Y.; Schief, W. R.; Hammond, P. T.; Irvine, D. J., Enhancing humoral immunity via sustained-release implantable microneedle patch vaccination. *Proc Natl Acad Sci U S A* **2019,** *116* (33), 16473-16478.

47. Cirelli, K. M.; Carnathan, D. G.; Nogal, B.; Martin, J. T.; Rodriguez, O. L.; Upadhyay, A. A.; Enemuo, C. A.; Gebru, E. H.; Choe, Y.; Viviano, F.; Nakao, C.; Pauthner, M. G.; Reiss, S.; Cottrell, C. A.; Smith, M. L.; Bastidas, R.; Gibson, W.; Wolabaugh, A. N.; Melo, M. B.; Cossette, B.; Kumar, V.; Patel, N. B.; Tokatlian, T.; Menis, S.; Kulp, D. W.; Burton, D. R.; Murrell, B.; Schief, W. R.; Bosinger, S. E.; Ward, A. B.; Watson, C. T.; Silvestri, G.; Irvine, D. J.; Crotty, S., Slow Delivery Immunization Enhances HIV Neutralizing Antibody and Germinal Center Responses via Modulation of Immunodominance. *Cell* **2019,** *177* (5), 1153-1171 e28.
48. Wu, Y.; Norberg, P. K.; Reap, E. A.; Congdon, K. L.; Fries, C. N.; Kelly, S. H.; Sampson, J. H.; Conticello, V. P.; Collier, J. H., A Supramolecular Vaccine Platform Based on alpha-Helical Peptide Nanofibers. *ACS Biomater Sci Eng* **2017,** *3* (12), 3128-3132.
49. Hudalla, G. A.; Modica, J. A.; Tian, Y. F.; Rudra, J. S.; Chong, A. S.; Sun, T.; Mrksich, M.; Collier, J. H., A self-adjuvanting supramolecular vaccine carrying a folded protein antigen. *Adv Healthc Mater* **2013,** *2* (8), 1114-9.
50. De Koker, S.; Hoogenboom, R.; De Geest, B. G., Polymeric multilayer capsules for drug delivery. *Chem Soc Rev* **2012,** *41* (7), 2867-84.
51. Appel, E. A.; Tibbitt, M. W.; Webber, M. J.; Mattix, B. A.; Veiseh, O.; Langer, R., Self-assembled hydrogels utilizing polymer-nanoparticle interactions. *Nat Commun* **2015,** *6*, 6295.
52. Appel, E. A.; del Barrio, J.; Loh, X. J.; Scherman, O. A., Supramolecular polymeric hydrogels. *Chem Soc Rev* **2012,** *41* (18), 6195-214.
53. Mann, J. L.; Yu, A. C.; Agmon, G.; Appel, E. A., Supramolecular polymeric biomaterials. *Biomater Sci* **2017,** *6* (1), 10-37.
54. Stapleton, L. M.; Steele, A. N.; Wang, H.; Lopez Hernandez, H.; Yu, A. C.; Paulsen, M. J.; Smith, A. A. A.; Roth, G. A.; Thakore, A. D.; Lucian, H. J.; Totherow, K. P.; Baker, S. W.; Tada, Y.; Farry, J. M.; Eskandari, A.; Hironaka, C. E.; Jaatinen, K. J.; Williams, K. M.; Bergamasco, H.; Marschel, C.; Chadwick, B.; Grady, F.; Ma, M.; Appel, E. A.; Woo, Y. J., Use of a supramolecular polymeric hydrogel as an effective post-operative pericardial adhesion barrier. *Nat Biomed Eng* **2019,** *3* (8), 611-620.
55. Appel, E. A.; Tibbitt, M. W.; Greer, J. M.; Fenton, O. S.; Kreuels, K.; Anderson, D. G.; Langer, R., Exploiting Electrostatic Interactions in Polymer–Nanoparticle Hydrogels. *ACS Macro Letters* **2015,** *4* (8), 848-852.
56. Gale, E. C.; Lahey, L. J.; Böhnert, V.; Powell, A. E.; Ou, B. S.; Carozza, J. A.; Li, L.; Appel, E. A., A cGAMP-containing hydrogel for prolonged SARS-CoV-2 RBD subunit vaccine exposure induces a broad and potent humoral response. Cold Spring Harbor Laboratory: 2021.
57. Gale, E. C.; Powell, A. E.; Roth, G. A.; Meany, E. L.; Yan, J.; Ou, B. S.; Grosskopf, A. K.; Adamska, J.; Picece, V. C. T. M.; D'Aquino, A. I.; Pulendran, B.; Kim, P. S.; Appel, E. A., Hydrogel-Based Slow Release of a Receptor-Binding Domain Subunit Vaccine Elicits Neutralizing Antibody Responses Against SARS-CoV-2. *Advanced Materials* **2021,** *33* (51), 2104362.
58. Maikawa, C. L.; Sevit, A.; Lin, B.; Wallstrom, R. J.; Mann, J. L.; Yu, A. C.; Waymouth, R. M.; Appel, E. A., Block copolymer composition drives function of self-assembled nanoparticles for delivery of small-molecule cargo. *J Polym Sci A Polym Chem* **2019,** *57* (12), 1322-1332.
59. Smith, A. A. A.; Gale, E. C.; Roth, G. A.; Maikawa, C. L.; Correa, S.; Yu, A. C.; Appel, E. A., Nanoparticles Presenting Potent TLR7/8 Agonists Enhance Anti-PD-L1 Immunotherapy in Cancer Treatment. *Biomacromolecules* **2020,** *21* (9), 3704-3712.

60. Klein, F.; Diskin, R.; Scheid, J. F.; Gaebler, C.; Mouquet, H.; Georgiev, I. S.; Pancera, M.; Zhou, T.; Incesu, R. B.; Fu, B. Z.; Gnanapragasam, P. N.; Oliveira, T. Y.; Seaman, M. S.; Kwong, P. D.; Bjorkman, P. J.; Nussenzweig, M. C., Somatic mutations of the immunoglobulin framework are generally required for broad and potent HIV-1 neutralization. *Cell* **2013,** *153* (1), 126-38.
61. Roth, G. A.; Saouaf, O. M.; Smith, A. A. A.; Gale, E. C.; Hernández, M. A.; Idoyaga, J.; Appel, E. A., Prolonged Codelivery of Hemagglutinin and a TLR7/8 Agonist in a Supramolecular Polymer–Nanoparticle Hydrogel Enhances Potency and Breadth of Influenza Vaccination. *ACS Biomaterials Science & Engineering* **2021**.
62. Jons, C. K.; Grosskopf, A. K.; Baillet, J.; Yan, J.; Klich, J. H.; Saouaf, O. M.; Appel, E. A., Yield-Stress and Creep Control Depot Formation and Persistence of Injectable Hydrogels Following Subcutaneous Administration. *Advanced Functional Materials* **2022**, 2203402.
63. Fenton, O. S.; Tibbitt, M. W.; Appel, E. A.; Jhunjhunwala, S.; Webber, M. J.; Langer, R., Injectable Polymer-Nanoparticle Hydrogels for Local Immune Cell Recruitment. *Biomacromolecules* **2019,** *20* (12), 4430-4436.
64. Klein, D. C. G.; Latz, E.; Espevik, T.; Stokke, B. T., Higher order structure of short immunostimulatory oligonucleotides studied by atomic force microscopy. *Ultramicroscopy* **2010,** *110* (6), 689-693.
65. Axpe, E.; Chan, D.; Offeddu, G. S.; Chang, Y.; Merida, D.; Hernandez, H. L.; Appel, E. A., A Multiscale Model for Solute Diffusion in Hydrogels. *Macromolecules* **2019,** *52* (18), 6889-6897.
66. Slifka, M. K.; Whitton, J. L., Clinical implications of dysregulated cytokine production. *J Mol Med (Berl)* **2000,** *78* (2), 74-80.
67. Tisoncik, J. R.; Korth, M. J.; Simmons, C. P.; Farrar, J.; Martin, T. R.; Katze, M. G., Into the eye of the cytokine storm. *Microbiol Mol Biol Rev* **2012,** *76* (1), 16-32.
68. Nabel, K. G.; Clark, S. A.; Shankar, S.; Pan, J.; Clark, L. E.; Yang, P.; Coscia, A.; McKay, L. G. A.; Varnum, H. H.; Brusic, V.; Tolan, N. V.; Zhou, G.; Desjardins, M.; Turbett, S. E.; Kanjilal, S.; Sherman, A. C.; Dighe, A.; LaRocque, R. C.; Ryan, E. T.; Tylek, C.; Cohen-Solal, J. F.; Darcy, A. T.; Tavella, D.; Clabbers, A.; Fan, Y.; Griffiths, A.; Correia, I. R.; Seagal, J.; Baden, L. R.; Charles, R. C.; Abraham, J., Structural basis for continued antibody evasion by the SARS-CoV-2 receptor binding domain. *Science* **2022,** *375* (6578), eabl6251.
69. Fornefett, J.; Krause, J.; Klose, K.; Fingas, F.; Hassert, R.; Benga, L.; Grunwald, T.; Muller, U.; Schrodl, W.; Baums, C. G., Comparative analysis of humoral immune responses and pathologies of BALB/c and C57BL/6 wildtype mice experimentally infected with a highly virulent Rodentibacter pneumotropicus (Pasteurella pneumotropica) strain. *BMC Microbiol* **2018,** *18* (1), 45.
70. Brazolot Millan, C. L.; Weeratna, R.; Krieg, A. M.; Siegrist, C. A.; Davis, H. L., CpG DNA can induce strong Th1 humoral and cell-mediated immune responses against hepatitis B surface antigen in young mice. *Proc Natl Acad Sci U S A* **1998,** *95* (26), 15553-8.
71. Mirotti, L.; Alberca Custódio, R. W.; Gomes, E.; Rammauro, F.; de Araujo, E. F.; Garcia Calich, V. L.; Russo, M., CpG-ODN Shapes Alum Adjuvant Activity Signaling via MyD88 and IL-10. *Frontiers in Immunology* **2017,** *8*.
72. Zimmermann, S.; Egeter, O.; Hausmann, S.; Lipford, G. B.; Röcken, M.; Wagner, H.; Heeg, K., Cutting Edge: CpG Oligodeoxynucleotides Trigger Protective and Curative Th1 Responses in Lethal Murine Leishmaniasis. *The Journal of Immunology* **1998,** *160* (8), 3627-3630.

73. Gil-Etayo, F. J.; Garcinuno, S.; Utrero-Rico, A.; Cabrera-Marante, O.; Arroyo-Sanchez, D.; Mancebo, E.; Pleguezuelo, D. E.; Rodriguez-Frias, E.; Allende, L. M.; Morales-Perez, P.; Castro-Panete, M. J.; Lalueza, A.; Lumbreras, C.; Paz-Artal, E.; Serrano, A., An Early Th1 Response Is a Key Factor for a Favorable COVID-19 Evolution. *Biomedicines* **2022,** *10* (2).
74. Gil-Etayo, F. J.; Suarez-Fernandez, P.; Cabrera-Marante, O.; Arroyo, D.; Garcinuno, S.; Naranjo, L.; Pleguezuelo, D. E.; Allende, L. M.; Mancebo, E.; Lalueza, A.; Diaz-Simon, R.; Paz-Artal, E.; Serrano, A., T-Helper Cell Subset Response Is a Determining Factor in COVID-19 Progression. *Front Cell Infect Microbiol* **2021,** *11*, 624483.
75. Axelrod, D.; Koppel, D. E.; Schlessinger, J.; Elson, E.; Webb, W. W., Mobility measurement by analysis of fluorescence photobleaching recovery kinetics. *Biophysical Journal* **1976,** *16* (9), 1055-1069.
76. Neuman, B. W.; Adair, B. D.; Yoshioka, C.; Quispe, J. D.; Orca, G.; Kuhn, P.; Milligan, R. A.; Yeager, M.; Buchmeier, M. J., Supramolecular architecture of severe acute respiratory syndrome coronavirus revealed by electron cryomicroscopy. *J Virol* **2006,** *80* (16), 7918-28.
77. Powell, A. E.; Zhang, K.; Sanyal, M.; Tang, S.; Weidenbacher, P. A.; Li, S.; Pham, T. D.; Pak, J. E.; Chiu, W.; Kim, P. S., A Single Immunization with Spike-Functionalized Ferritin Vaccines Elicits Neutralizing Antibody Responses against SARS-CoV-2 in Mice. *ACS Central Science* **2021,** *7* (1), 183-199.

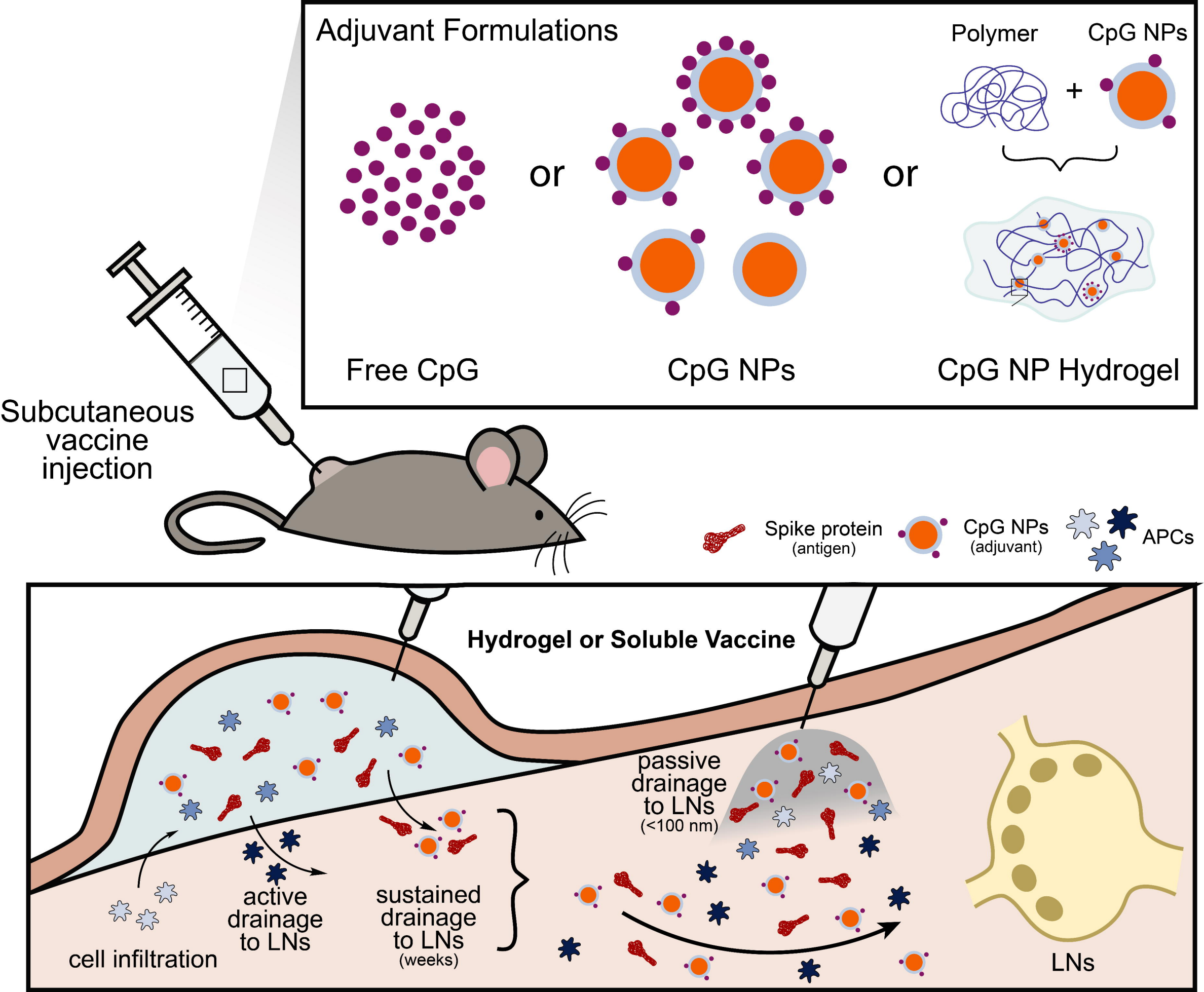
Adjuvant Formulations
Polymer
CpG NPs
+
or
or
Free CpG
CpG NPs
CpG NP Hydrogel
Subcutaneous vaccine injection
Spike protein (antigen)
CpG NPs (adjuvant)
APCs
Hydrogel or Soluble Vaccine
passive drainage to LNs (<100 nm)
active drainage to LNs
sustained drainage to LNs (weeks)
cell infiltration
LNs

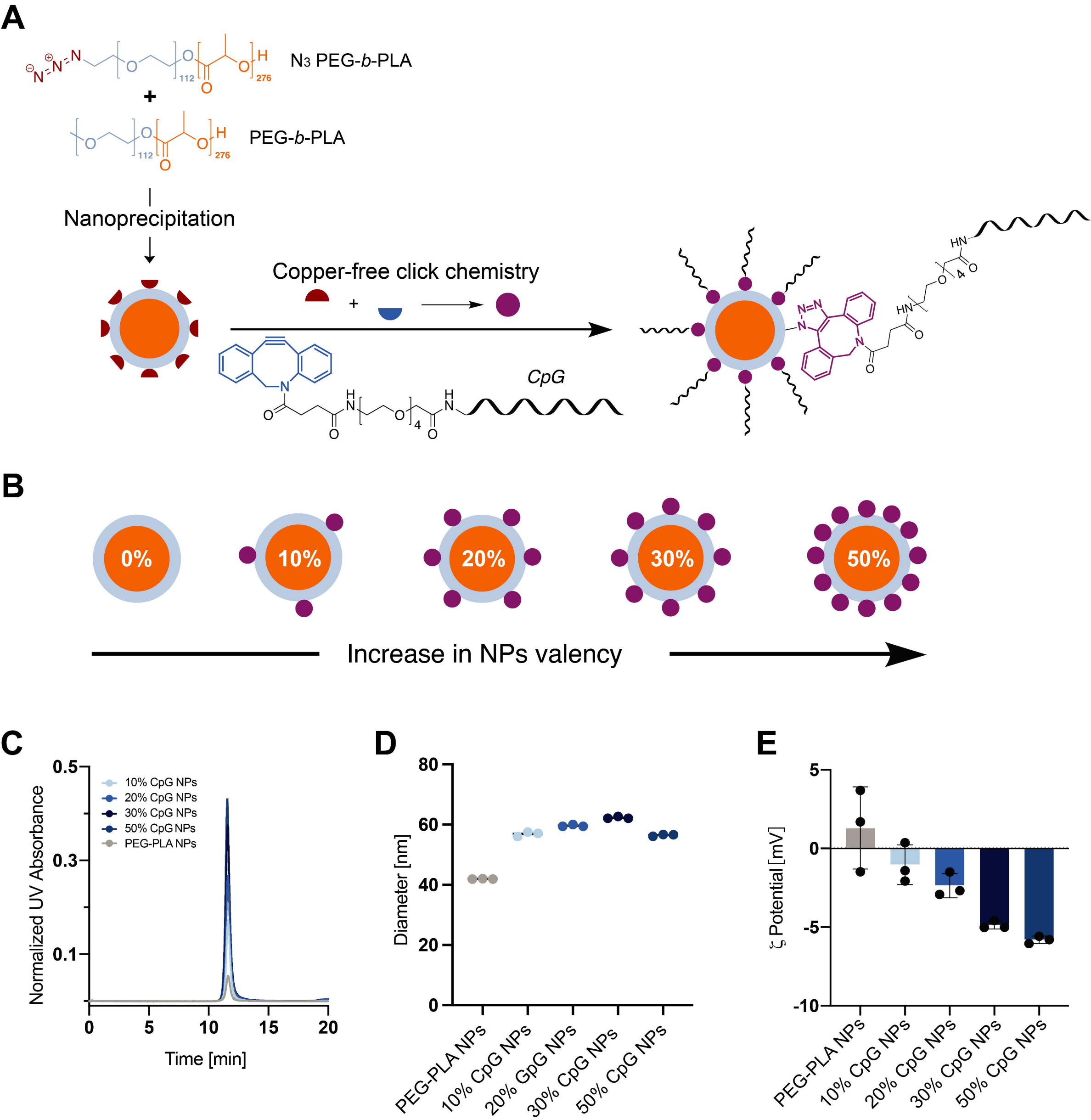
A
N3 PEG-b-PLA
PEG-b-PLA
Nanoprecipitation
Copper-free click chemistry
CpG
B
0%
10%
20%
30%
50%
Increase in NPs valency
C
Normalized UV Absorbance
Time [min]
10% CpG NPs
20% CpG NPs
30% CpG NPs
50% CpG NPs
PEG-PLA NPs
D
Diameter [nm]
PEG-PLA NPs
10% CpG NPs
20% GpG NPs
30% CpG NPs
50% CpG NPs
E
ζ Potential [mV]
PEG-PLA NPs
10% CpG NPs
20% CpG NPs
30% CpG NPs
50% CpG NPs

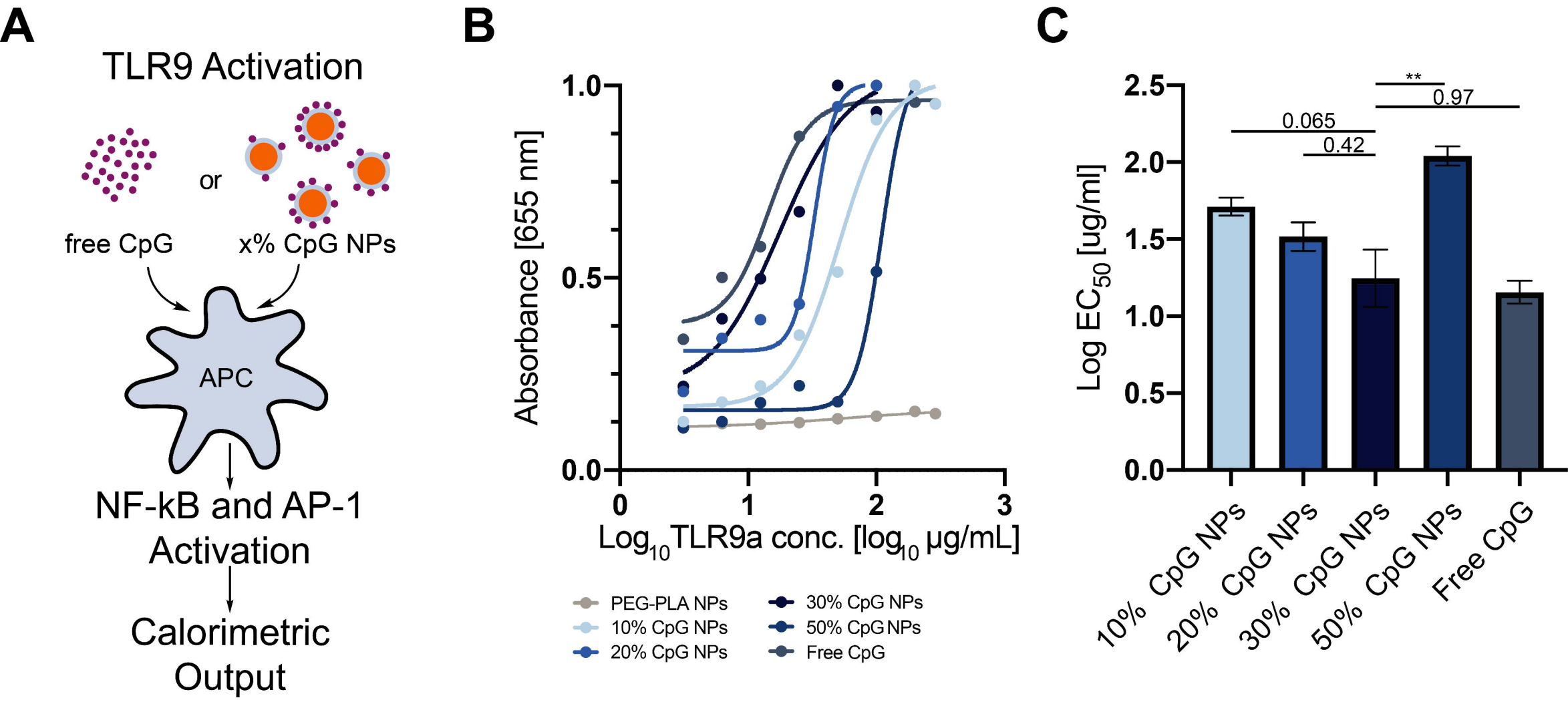
A
TLR9 Activation
or
free CpG
x% CpG NPs
APC
NF-kB and AP-1 Activation
Calorimetric Output
B
Absorbance [655 nm]
1.0
0.5
0.0
0
1
2
3
Log10TLR9a conc. [log10 µg/mL]
PEG-PLA NPs
10% CpG NPs
20% CpG NPs
30% CpG NPs
50% CpG NPs
Free CpG
C
Log EC50 [ug/ml]
2.5
2.0
1.5
1.0
0.5
0.0
**
0.97
0.065
0.42
10% CpG NPs
20% CpG NPs
30% CpG NPs
50% CpG NPs
Free CpG

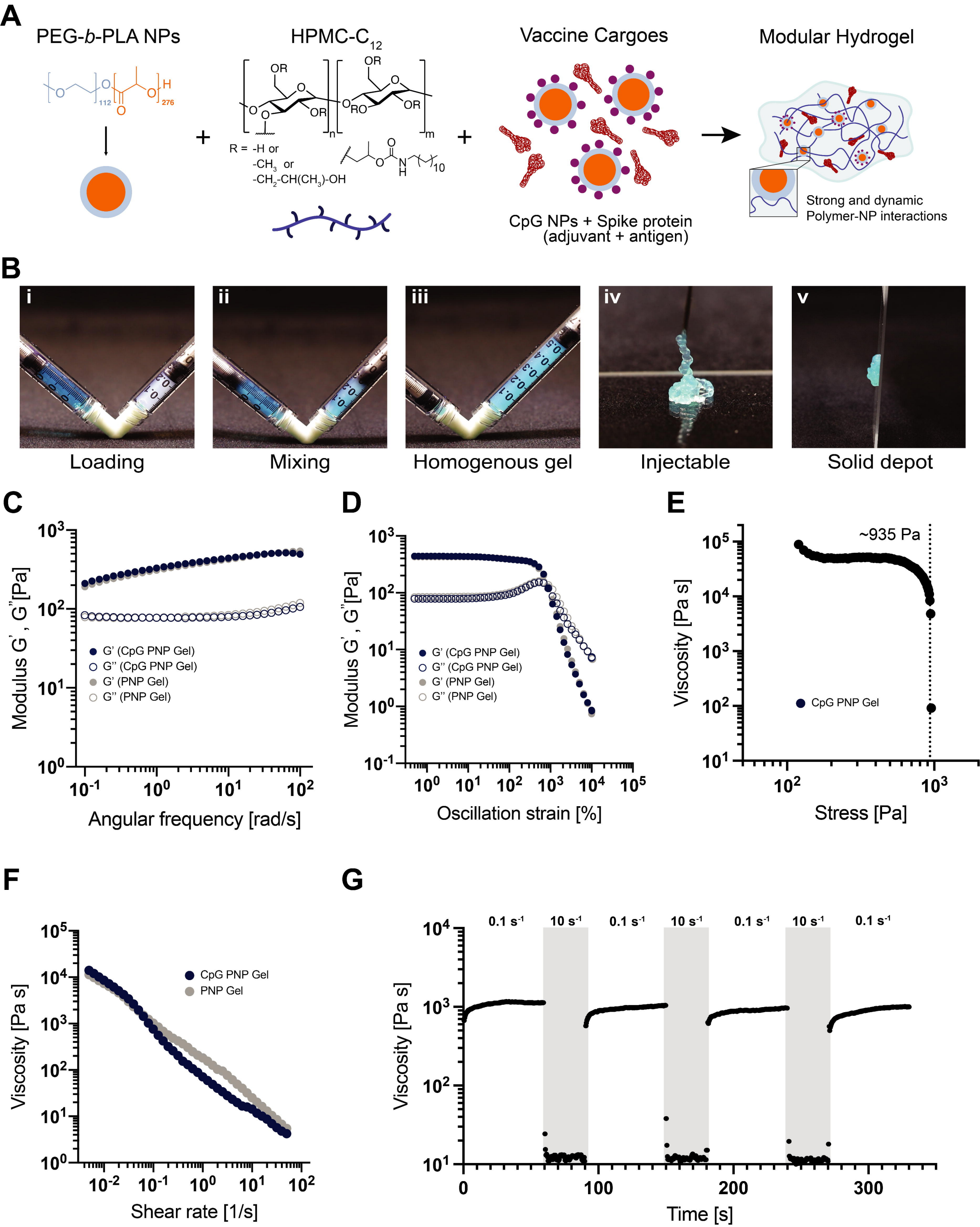
A
PEG-b-PLA NPs
HPMC-C12
Vaccine Cargoes
Modular Hydrogel
R = -H or
-CH3 or
-CH2-CH(CH3)-OH
CpG NPs + Spike protein
(adjuvant + antigen)
Strong and dynamic
Polymer-NP interactions
B
i
ii
iii
iv
v
Loading
Mixing
Homogenous gel
Injectable
Solid depot
C
Modulus G', G''[Pa]
Angular frequency [rad/s]
G' (CpG PNP Gel)
G'' (CpG PNP Gel)
G' (PNP Gel)
G'' (PNP Gel)
D
Modulus G', G''[Pa]
Oscillation strain [%]
G' (CpG PNP Gel)
G'' (CpG PNP Gel)
G' (PNP Gel)
G'' (PNP Gel)
E
~935 Pa
Viscosity [Pa s]
Stress [Pa]
CpG PNP Gel
F
Viscosity [Pa s]
Shear rate [1/s]
CpG PNP Gel
PNP Gel
G
0.1 s-1
10 s-1
0.1 s-1
10 s-1
0.1 s-1
10 s-1
0.1 s-1
Viscosity [Pa s]
Time [s]

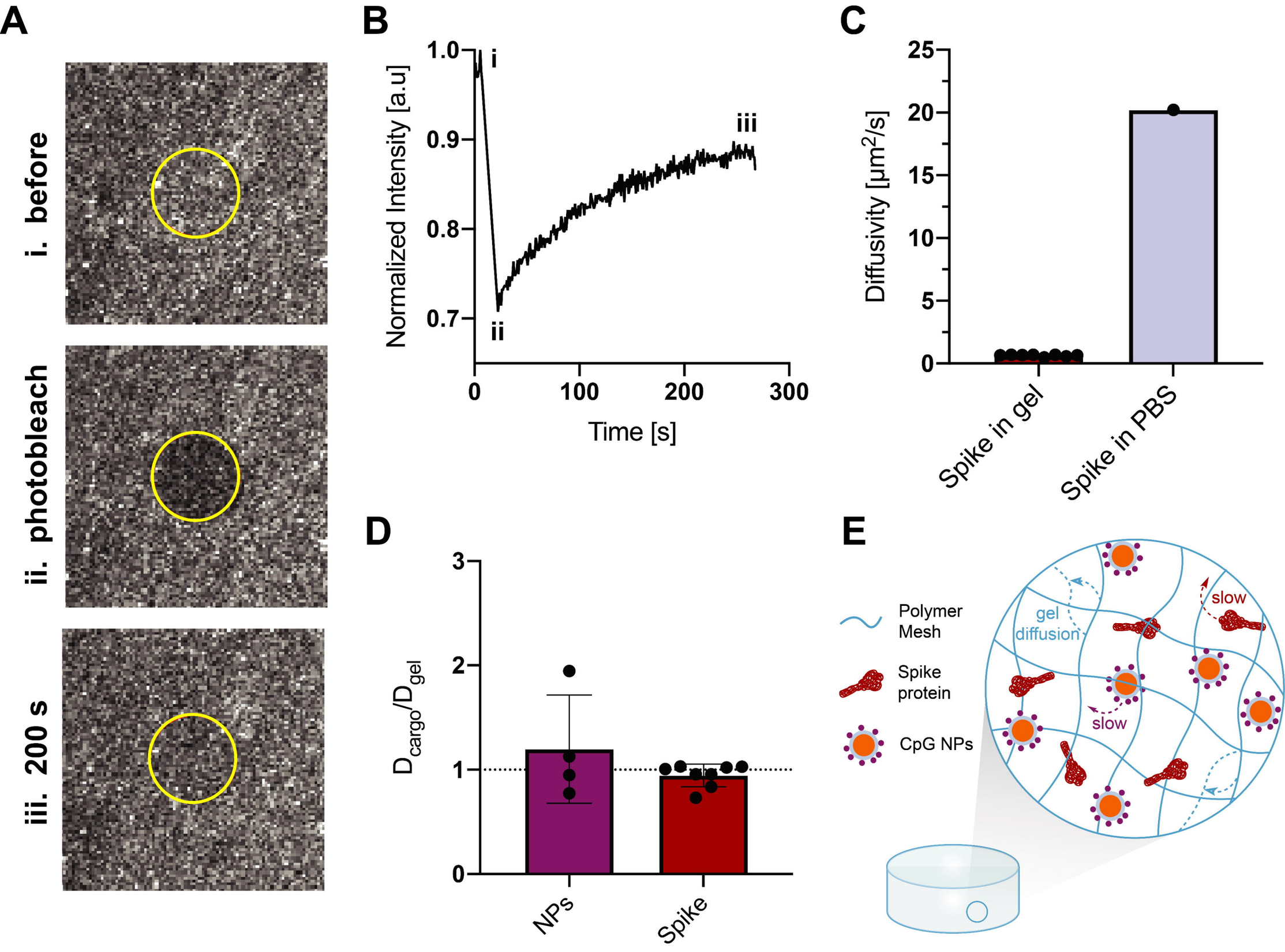
A
i. before
ii. photobleach
iii. 200 s
B
Normalized Intensity [a.u]
1.0
0.9
0.8
0.7
i
ii
iii
0
100
200
300
Time [s]
C
Diffusivity [μm²/s]
25
20
15
10
5
0
Spike in gel
Spike in PBS
D
D_cargo/D_gel
3
2
1
0
NPs
Spike
E
Polymer Mesh
Spike protein
CpG NPs
gel diffusion
slow
slow

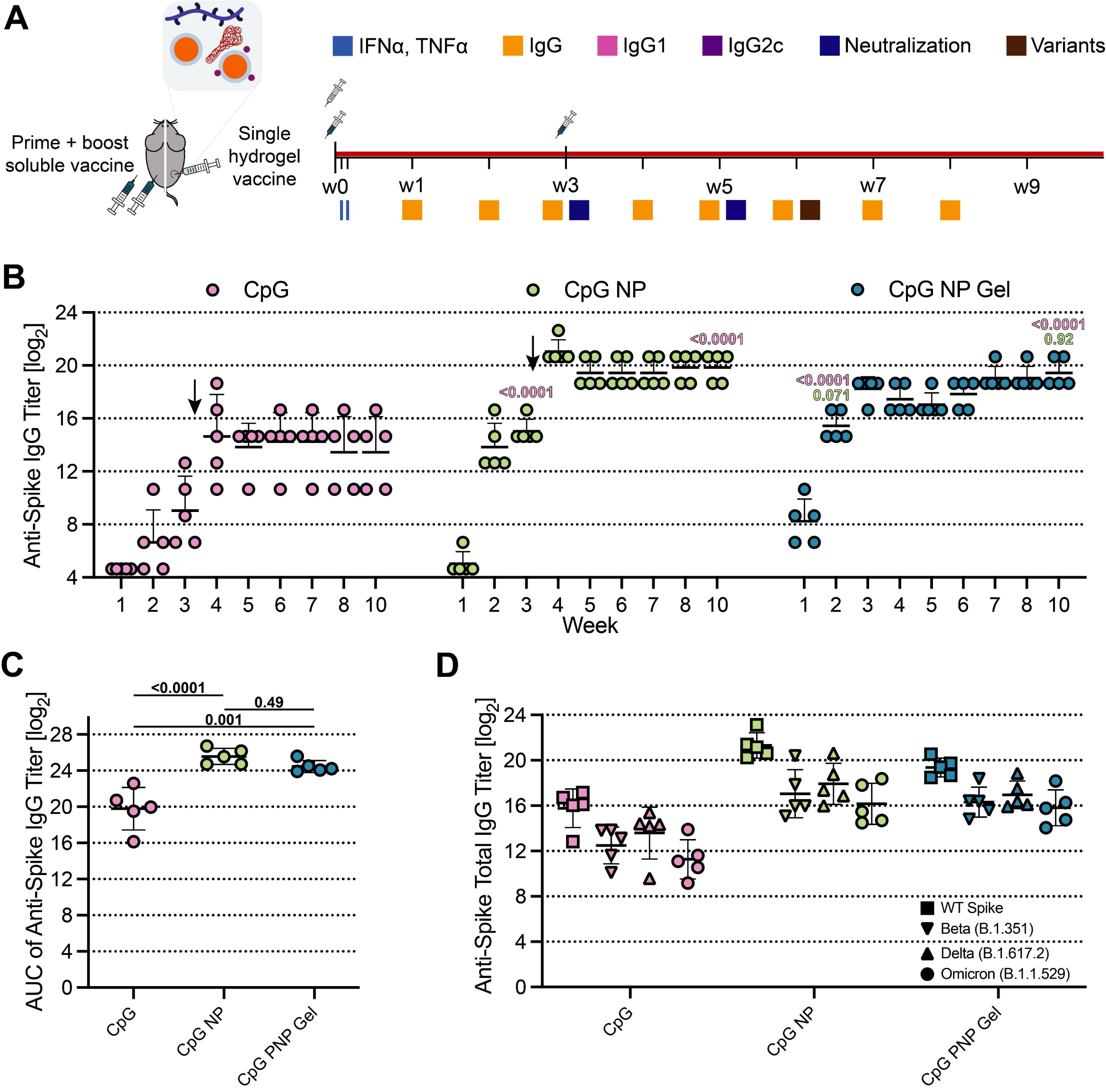
A
IFNα, TNFα
IgG
IgG1
IgG2c
Neutralization
Variants
Prime + boost soluble vaccine
Single hydrogel vaccine
w0
w1
w3
w5
w7
w9
B
CpG
CpG NP
CpG NP Gel
Anti-Spike IgG Titer [log2]
<0.0001
<0.0001
<0.0001
0.071
<0.0001
0.92
Week
C
AUC of Anti-Spike IgG Titer [log2]
<0.0001
0.49
0.001
CpG
CpG NP
CpG PNP Gel
D
Anti-Spike Total IgG Titer [log2]
WT Spike
Beta (B.1.351)
Delta (B.1.617.2)
Omicron (B.1.1.529)
CpG
CpG NP
CpG PNP Gel

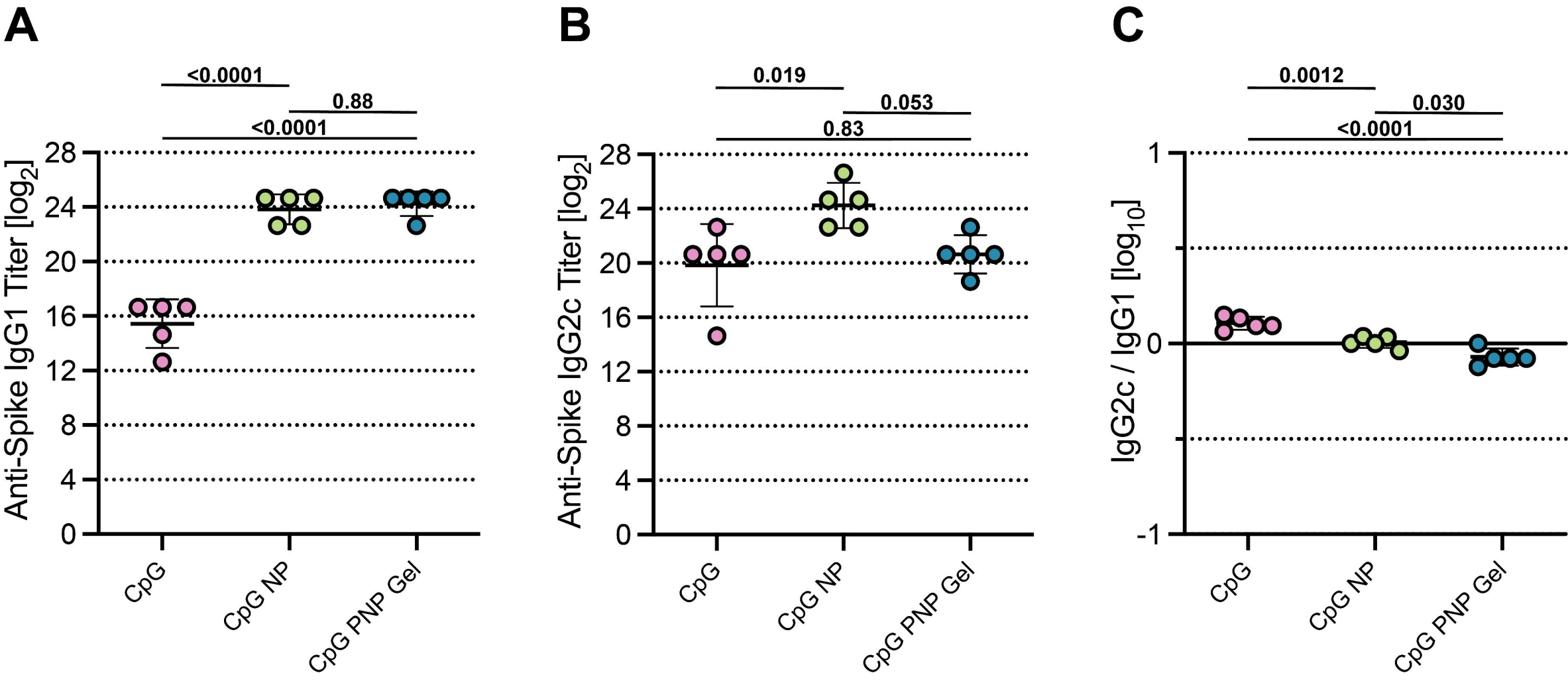
A
<0.0001
0.88
<0.0001
Anti-Spike IgG1 Titer [log2]
28
24
20
16
12
8
4
0
CpG
CpG NP
CpG PNP Gel
B
0.019
0.053
0.83
Anti-Spike IgG2c Titer [log2]
28
24
20
16
12
8
4
0
CpG
CpG NP
CpG PNP Gel
C
0.0012
0.030
<0.0001
IgG2c / IgG1 [log10]
1
0
-1
CpG
CpG NP
CpG PNP Gel

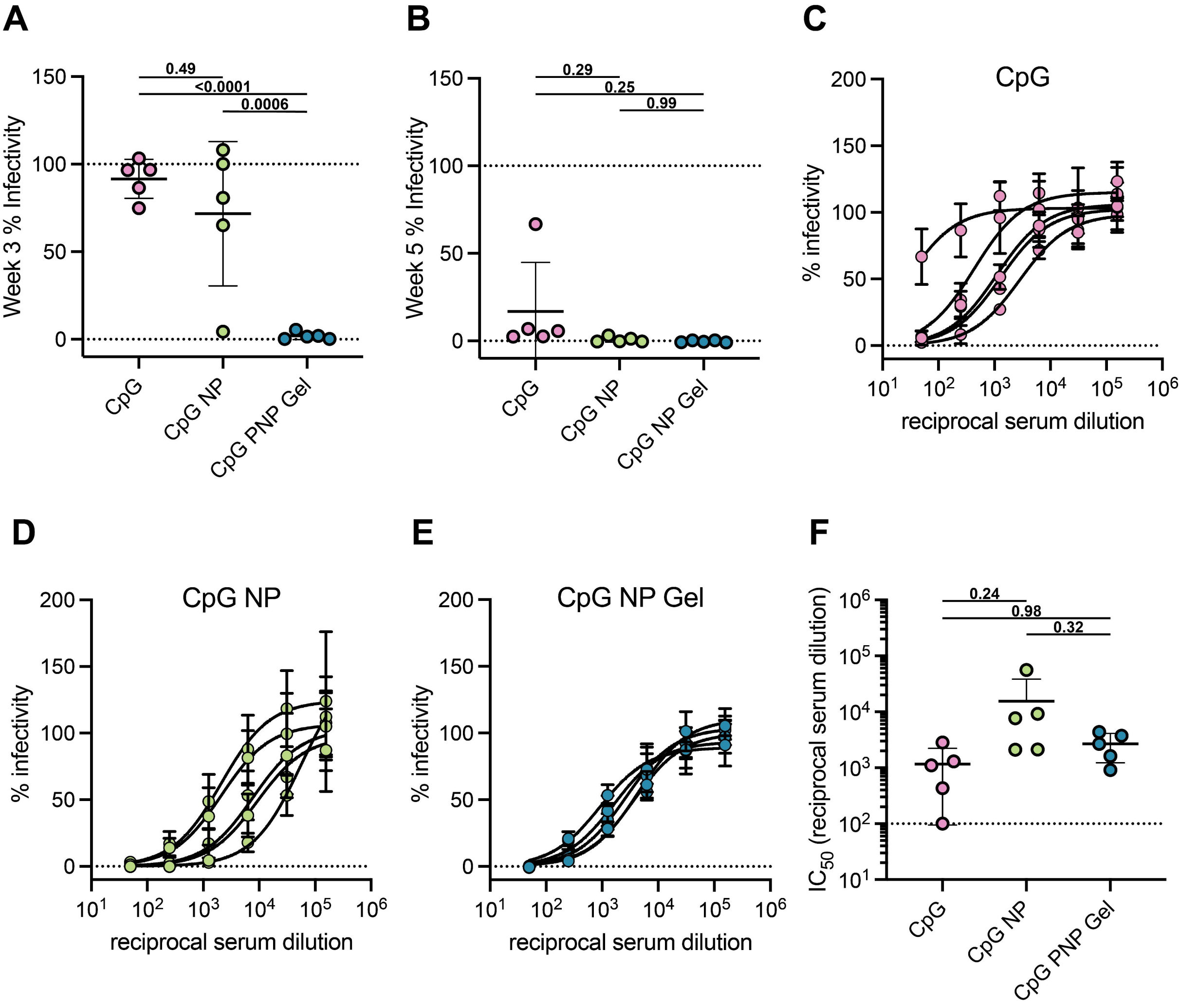
A
Week 3 % Infectivity
150
100
50
0
0.49
<0.0001
0.0006
CpG
CpG NP
CpG PNP Gel
B
Week 5 % Infectivity
150
100
50
0
0.29
0.25
0.99
CpG
CpG NP
CpG NP Gel
C
CpG
% infectivity
200
150
100
50
0
10^1 10^2 10^3 10^4 10^5 10^6
reciprocal serum dilution
D
CpG NP
% infectivity
200
150
100
50
0
10^1 10^2 10^3 10^4 10^5 10^6
reciprocal serum dilution
E
CpG NP Gel
% infectivity
200
150
100
50
0
10^1 10^2 10^3 10^4 10^5 10^6
reciprocal serum dilution
F
IC_{50} (reciprocal serum dilution)
10^6
10^5
10^4
10^3
10^2
10^1
0.24
0.98
0.32
CpG
CpG NP
CpG PNP Gel